Article

Cell Host & Microbe

A Ribose-Scavenging System Confers Colonization Fitness on the Human Gut Symbiont *Bacteroides thetaiotaomicron* in a Diet-Specific Manner

Graphical Abstract

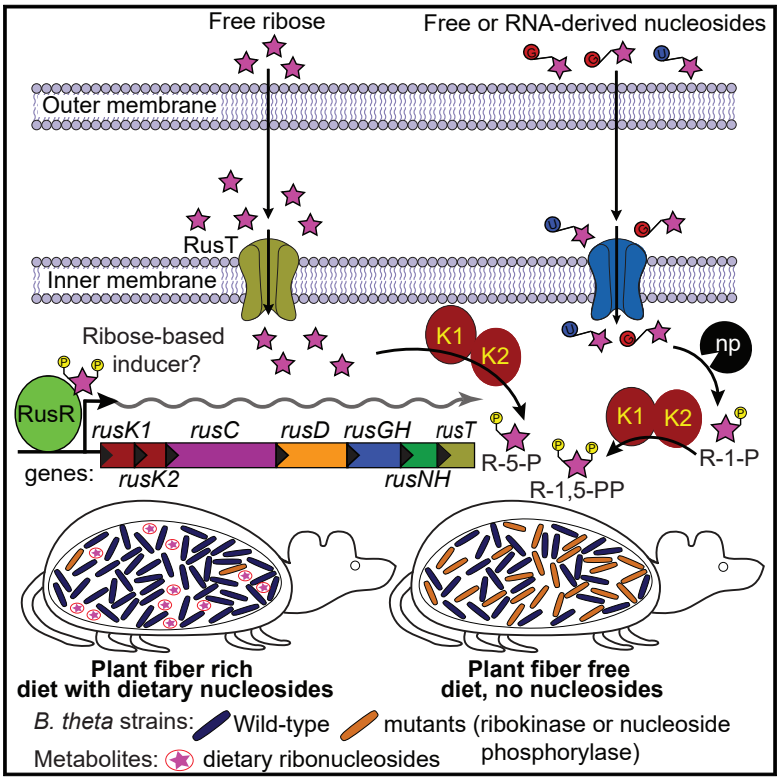

Highlights

- Human gut Bacteroidetes and their relatives have diverse ribose-scavenging systems
- A *B. thetaiotaomicron* ribose-utilization system (RUS) is needed on a plant diet
- RUS ribokinases are the critical diet-specific determinants
- Ribokinases yield ribose-1,5-bisphosphate from cleaved product of an unlinked gene

Authors

Robert W.P. Glowacki, Nicholas A. Pudlo, Yunus Tuncil, ..., Costas A. Lyssiotis, Bruce R. Hamaker, Eric C. Martens

Correspondence

emartens@umich.edu

In Brief

Glowacki et al. show that the ability of *Bacteroides thetaiotaomicron* to use ribose derived from nucleosides is an important function *in vivo* on a plant-fiber-rich diet. Ribokinases encoded in a ribose-utilization system (RUS) and an unlinked nucleoside phosphorylase mediate this effect *in vivo* through generation of ribose-1,5-bisphosphate.

Glowacki et al., 2020, Cell Host & Microbe *27*, 79–92
January 8, 2020
https://doi.org/10.1016/j.chom.2019.11.009

CellPress

Cell Host & Microbe
Article

A Ribose-Scavenging System Confers Colonization Fitness on the Human Gut Symbiont *Bacteroides thetaiotaomicron* in a Diet-Specific Manner

Robert W.P. Glowacki,[1] Nicholas A. Pudlo,[1] Yunus Tuncil,[2,4] Ana S. Luis,[1,5] Peter Sajjakulnukit,[3] Anton I. Terekhov,[2] Costas A. Lyssiotis,[3] Bruce R. Hamaker,[2] and Eric C. Martens[1,6,*]
[1]Department of Microbiology and Immunology, University of Michigan Medical School, Ann Arbor, MI 48109, USA
[2]Department of Food Science and Whistler Center for Carbohydrate Research, Purdue University, West Lafayette, IN 47907, USA
[3]Department of Molecular and Integrative Physiology, University of Michigan Medical School, Ann Arbor, MI 48109, USA
[4]Present address: Department of Food Engineering, Ordu University, Ordu, Turkey
[5]Present address: Department of Medical Biochemistry and Cell Biology, Institute of Biomedicine, University of Gothenburg, Gothenburg, Sweden
[6]Lead Contact
*Correspondence: emartens@umich.edu
https://doi.org/10.1016/j.chom.2019.11.009

SUMMARY

Efficient nutrient acquisition in the human gut is essential for microbial persistence. Although polysaccharides have been well-studied nutrients for the gut microbiome, other resources such as nucleic acids and nucleosides are less studied. We describe several ribose-utilization systems (RUSs) that are broadly represented in Bacteroidetes and appear to have diversified to access ribose from a variety of substrates. One *Bacteroides thetaiotaomicron* RUS variant is critical for competitive gut colonization in a diet-specific fashion. We used molecular genetics to probe the required functions of the system and the nature of the nutrient source(s) underlying this phenotype. Two RUS-encoded ribokinases were the only components required for this effect, presumably because they generate ribose-phosphate derivatives from products of an unlinked but essential nucleoside phosphorylase. Our results underscore the extensive mechanisms that gut symbionts have evolved to access nutrients and the potential for unexpected dependencies among systems that mediate colonization and persistence.

INTRODUCTION

Symbiotic microorganisms that inhabit the human intestine complement digestive capacity in numerous ways, the most mechanistically understood examples of which involve degradation of diverse dietary polysaccharides (Porter and Martens, 2017). In contrast, the digestive fates of nucleic acids (from diet, host, or microbial origin) and their component ribo- and deoxyribonucleosides are less understood, as are their contributions to gut-microbiota community structure and physiology. Mutualistic *Lactobacillus* (McLeod et al., 2011) and *Bifidobacterium* (Pokusaeva et al., 2010) and pathogenic and non-pathogenic *Escherichia coli* (Fabich et al., 2008) and *Salmonella enterica* (Harvey et al., 2011) have characterized ribose-degrading systems. Additional systems containing nucleoside-cleaving enzymes have been defined in *E. coli* and fecal isolates of *Corynebacterium* (Hammer-Jespersen et al., 1971; Kim et al., 2006). In *E. coli*, DNA can serve as a sole carbon source through the action of competence genes and exonucleases (Finkel and Kolter, 2001; Palchevskiy and Finkel, 2009). Mechanisms for assimilating exogenous RNA have not been explored.

Members of the phylum *Bacteroidetes* constitute a major portion of bacteria in the human gut; individual species devote large portions of their genomes toward carbohydrate utilization via coordinately regulated polysaccharide utilization loci (PULs). A number of these PULs targeting dietary polysaccharides from plant cell walls or fermented foods have been thoroughly characterized (Cuskin et al., 2015; Larsbrink et al., 2014; Luis et al., 2018; Ndeh et al., 2017; Rogowski et al., 2015). Other characterized PULs are involved in the degradation of infrequent dietary substrates such as agarose and porphyran in edible seaweed (Hehemann et al., 2012; Pluvinage et al., 2018) or host-derived glycans such as those in mucus (Briliūtė et al., 2019; Martens et al., 2008). Despite variations in the substrates they target, the cellular systems encoded by Bacteroidetes PULs are similarly patterned to the prototypic starch utilization system (Sus)—each contains one or more TonB-dependent receptors (SusC homologs) and corresponding substrate-binding lipoproteins (SusD homologs). These two proteins form a complex (Glenwright et al., 2017) and work in concert with a variable repertoire of carbohydrate-degrading enzymes, substrate-binding proteins, and regulators to bind, degrade, and import substrates. Despite these studies, many identified PULs within genomes of gut and environmental Bacteroidetes lack existing knowledge of their target substrates (Terrapon et al., 2018), suggesting that they have evolved to target a broader range of nutrients beyond the common plant and host polysaccharides that have been evaluated (Martens et al., 2011; McNulty et al., 2013).

Here, we describe a ribose-responsive PUL in the human gut symbiont *Bacteroides thetaiotaomicron* (*Bt*). Variants of this

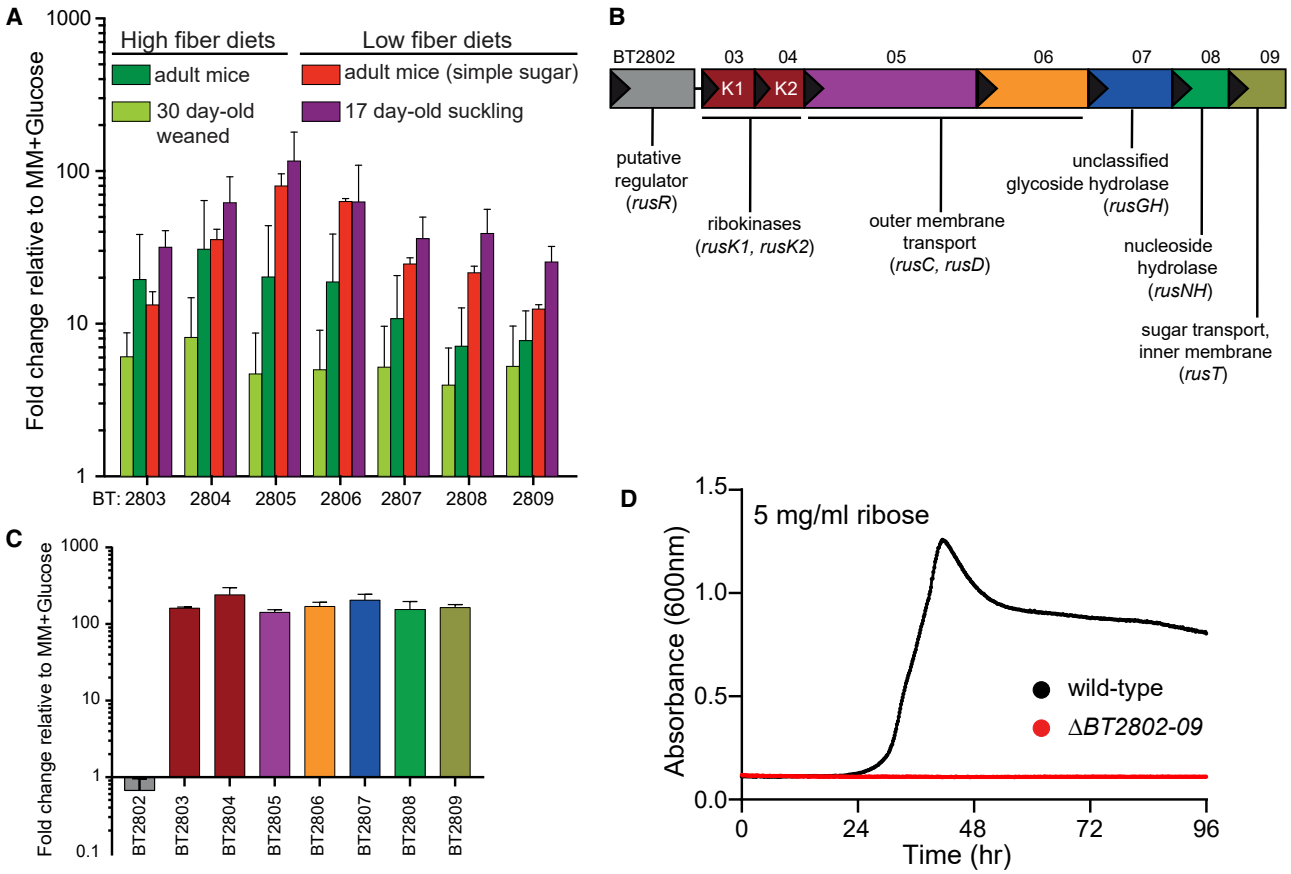

Figure 1. *Bt* Upregulates a PUL for Ribose Metabolism *In Vivo* and *In Vitro* in Response to Ribose

(A) *In vivo* Genechip data showing fold change in relation to *in vitro* growth MM, plus glucose for *BT2803–2809* in mice fed high-fiber diets (dark- and light-green bars for adult and 30-day-old weaned mice, respectively) and low-fiber diets (red and purple bars for adult and 17-day-old suckling mice, respectively).

(B) Organization of the *rus* locus with locus tag numbers, names, and predicted functions.

(C) *In vitro* transcriptional response of *Bt rus* genes in MM-ribose in comparison with MM-glucose reference (n = 3; error bars are SD of the mean).

(D) Growth in MM ribose (5 mg/mL) for wild-type *Bt* (black) or a strain lacking *rus* (red) (minimum of n = 5 separate replicates).

PUL exist in a diverse range of human gut and environmental Bacteroidetes but on the basis of enzymatic diversity have most likely evolved to target a variety of different ribose-containing nutrients. Using *Bt* as a model, we investigated the functions of this PUL *in vivo* in multiple diet conditions and *in vitro* in defined media. We show that this PUL is essential for utilization of ribose through the activity of two ribokinases, enzymes that catalyze formation of ribose-5-phosphate from ribose or ribose-1,5-bisphosphate from the product of a genomically unlinked nucleoside phosphorylase that is required for growth on nucleosides. The ability to catabolize ribose through PUL-encoded functions and the unlinked nucleoside phosphorylase confers a strong, diet-specific competitive advantage to *Bt in vivo.* This suggests a model in which a diet-specific nucleoside-scavenging pathway has become dependent on cellular ribokinases, which are critical for creating phosphorylated ribose intermediates and are persistently activated in the gut by an unknown signal. Our results reveal that a variety of host-associated and terrestrial bacteria have evolved mechanisms to scavenge ribose and nucleosides that are important for colonization. The common regulation of a family of highly diversified PULs by ribose, which occurs in nucleic acids, co-factors, modifications (ADP- and poly-ADP-ribose), bacteriocins, and bacterial capsules, suggests that these systems have adapted at the level of encoded enzymes to release ribose from varied sources, thus diversifying the nutrient niches available to these bacteria. However, the results of our *in vivo* studies highlight that underlying mechanisms for observed colonization advantages are context specific and not always directly attributable to the most obvious function performed or predicted by a particular system.

RESULTS

A Ribose-Inducible Gene Cluster Is Highly Active *In Vivo* and Required for Fitness in a Diet-Dependent Fashion

Members of the human gut Bacteroidetes typically encode coordinated degradative functions within discrete PULs, facilitating identification of components that work together to access particular nutrients (Martens et al., 2009). Previous work using gnotobiotic mice colonized with only *Bt* identified one such locus (*BT2803–2809*) for which all individual genes are upregulated between 10- and 139-fold in mice fed high- or low-fiber diets

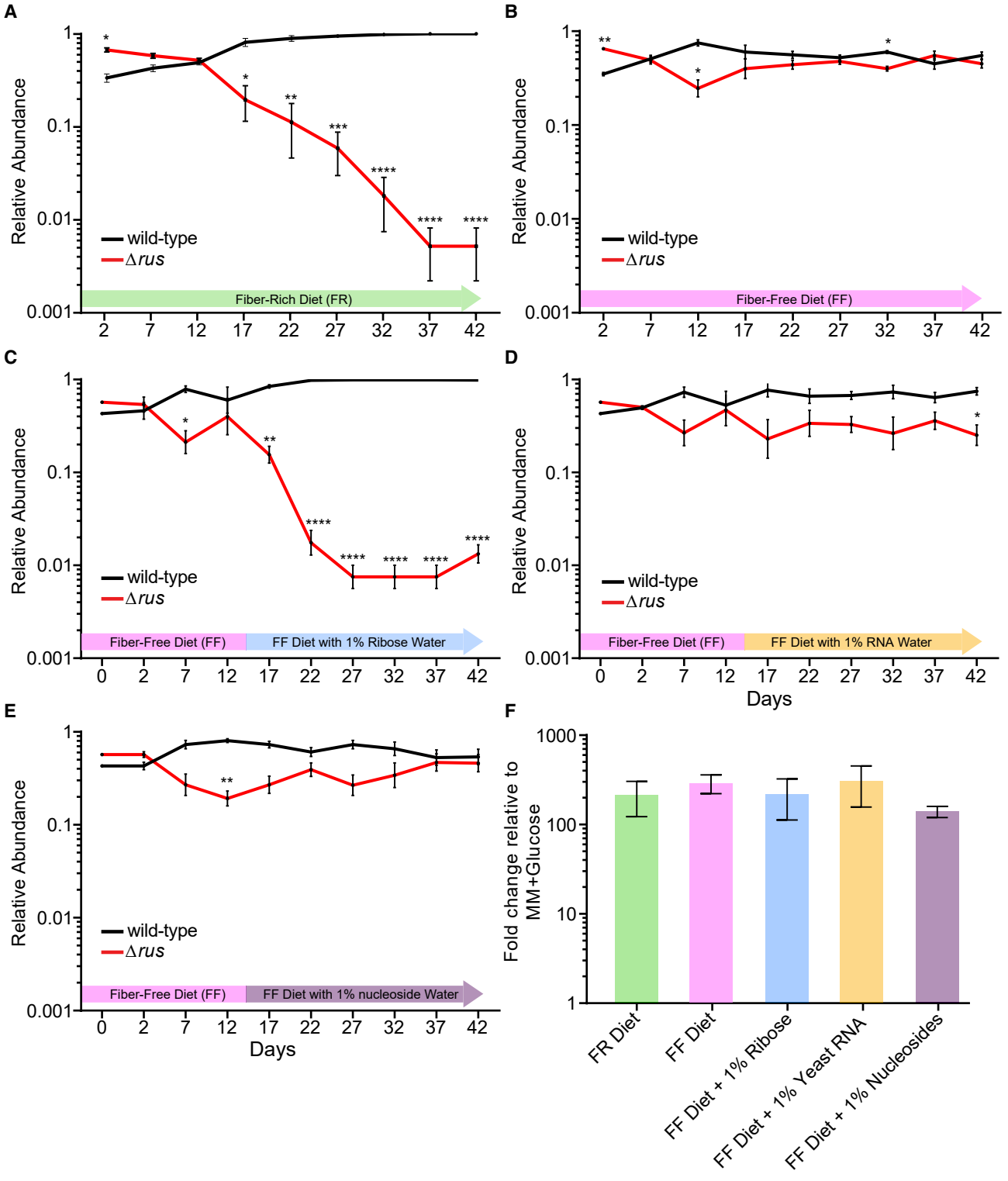

Figure 2. The *Bt rus* Locus Confers a Competitive Advantage *In Vivo* in a Diet-Dependent Context

(A–E) Log-scale relative abundance of wild-type (black line) and Δ*rus* (red line) strains enumerated by qRT-PCR from feces of 6- to 8-week-old germfree Swiss-Webster mice.

(A) Mice fed a high-fiber diet (green arrow; n = 4 mice).

(B) Mice pre-fed a FF diet for 1 week prior to colonization and maintained for 42 days (pink arrow).

(legend continued on next page)

(Figure 1A). During low fiber, *Bt*'s physiology shifts to expression of genes involved in host glycan foraging (Bjursell et al., 2006; Martens et al., 2008; Sonnenburg et al., 2005). Thus, expression of *BT2803–2809* in the absence of dietary fiber suggested that it could also target endogenous nutrients.

Typically, PULs involved in host glycan foraging encode enzymes required for liberating sugars from mucins and other glycoconjugates (fucosidases, sulfatases, etc.), but the content of the *BT2803–2809* PULs was different in several ways (Figure 1B). Three predicted enzymes (one nucleoside hydrolase and two ribokinases) suggested a role in assimilating ribose from substrate(s) such as nucleosides. A previous study determined that *Bt* grows on ribose (Martens et al., 2011), but the genes involved, relevant source(s) of ribose, and whether enzymatic liberation is required from complex substrates were not explored. The immediate upstream gene (*BT2802*) is predicted to have DNA-binding motifs and could act as a regulator, but the gene shares no homology to regulators previously associated with PULs. In addition to the enzymes noted above, other PUL genes encode homologs of the *Bacteroides* SusC and SusD outer-membrane proteins (*BT2805*, *BT2806*), a glycoside hydrolase of unassigned family and function (*BT2807*), a predicted nucleoside hydrolase (*BT2808*), and a sugar permease (*BT2809*).

The enzymes encoded in this PUL suggested the hypothesis that it is responsible for *Bt*'s ability to catabolize ribose and possibly liberate it from more complex sources such as nucleosides. To test whether this gene cluster is transcriptionally responsive to growth on ribose, we performed *in vitro* growth in minimal medium (MM) that contains ribose as the sole carbon source and measured expression of *BT2803–2809*. All genes were activated 142- to 240-fold during growth on ribose as compared to growth on glucose (Figure 1C). Other mono- and disaccharides did not activate this PUL as sole carbon sources (Figure S1A). We next examined the requirement for this locus by deleting *BT2802–2809*. Loss of the PUL eliminated growth on free ribose (Figure 1D) but did not affect growth on non-ribose substrates (Table S1). On the basis of these findings, we classified this PUL as the *Bt* ribose-utilization system, *rus*, and listed gene annotations in Figure 1B.

Because *rus* exhibits high transcriptional activity in the gnotobiotic mouse gut and is elevated in fiber-starved mice, we next hypothesized that the ability to utilize endogenous sources of ribose is advantageous *in vivo* during fiber-deficient diets. To test this, we inoculated 6- to 8-week-old germfree (GF) female Swiss-Webster mice with an equal mixture of wild-type and Δ*rus Bt* strains and maintained mice on either a fiber-rich (FR) diet containing several unprocessed plant-derived fiber polysaccharides or an accessible fiber-free (FF) diet consisting mainly of glucose, protein, lipids, and cellulose (Desai et al., 2016). With qPCR, we measured the relative abundance of each strain for 42 days in DNA extracted from feces. In opposition to our initial hypothesis, the Δ*rus* strain was strongly outcompeted (~100-fold) in mice fed the FR diet (Figure 2A). In contrast, in mice fed the FF diet, Δ*rus* exhibited similar abundance to wild-type *Bt* (Figure 2B). A similar competitive defect of the Δ*rus* strain in mice fed the FR diet was observed in separate experiments with 12-week-old female and 6- to 8-week-old male mice (Figures S1B and S1C), suggesting that the effect is not influenced by sex or age within the range tested. The FR-diet-associated defect was not a result of a lack of colonization or persistence because the levels of each strain were similar over time in mice colonized with either strain alone (Figures S1D and S1E). Additionally, the defect in the FR diet could not be attributed to the wild-type strain exhibiting different expression of the *rus* PUL because wild-type *Bt* exhibited similarly high levels of *rus* expression in mice fed either diet when present alone or in competition with the Δ*rus* mutant (Figure S1F).

Gas chromatography-mass spectrometry (GC-MS) analysis of the diets revealed ribose present only in the FR diet, at levels similar to those of other common monosaccharides, in an acid-hydrolyzable (i.e., covalently linked) but not free form. This suggested the presence of a ribose-containing molecule(s), such as RNA, nucleosides, or cofactors (Figure S2A). In cecal contents of FR-diet-fed mice mono-colonized with wild-type *Bt* or Δ*rus* strains, ribose was not detectable above our limit of detection (LOD) (Figure S2B). However, the LOD for ribose in the cecal contents was near the amount observed in the uneaten FR diet, raising the possibility that substantial amounts reach the cecum but are obscured. This ambiguity about the amount of diet-derived ribose *in vivo* prompted us to test whether different sources of dietary ribose affect *Bt* in the gut. We colonized three separate groups of GF mice with a mixture of wild-type and Δ*rus* strains and maintained them on the FF diet. After 14 days of stable competition between strains, water was supplemented with 1% ribose, 1% RNA, or 1% pyrimidine nucleosides (purines were not tested because of insolubility). The results clearly show that free ribose in the water exerts an effect against the Δ*rus* strain similar in magnitude to the defect in mice fed the FR diet (Figure 2C). Little or no defect was observed in mice provided water containing RNA or nucleosides (Figures 2D and 2E) even though increased acid-hydrolyzable ribose was detectable in the cecum (Figure S2C). There was comparable expression of the *rus* locus in all conditions, suggesting that *rus* expression differences did not account for different fitness outcomes (Figure 2F).

A Subset of Ribose-Utilization Functions Is Required for Competitive Colonization in Mice

The experiments described so far used a mutant lacking all eight *rus* genes, but only a subset of the functions might be important for competition. We therefore took a molecular genetic approach to more precisely probe the required functions and get a clearer idea of the nature of the important nutrient(s) in the FR diet. We constructed single and double gene deletions on the basis of

(C–E) Same diet and strain competition as in (B), but mice were given water containing 1% weight per volume (w/v) ribose (C), 1% w/v RNA from type IV Torula yeast tRNAs (D), or a 1% w/v mixture of nucleosides (0.25% each of uridine, cytidine, thymidine, and 5-methyl uridine) (E). The period of water supplementation is shaded blue, orange, or purple.

(F) *rusC* transcript levels measured by qRT-PCR from cecal contents of mice in (A)–(E).

In (A)–(F), the mean ± SEM is shown at each time point. In (A)–(E), asterisks indicate significant differences (*$p < 0.05$, **$p < 0.01$, ***$p < 0.001$, and ****$p < 0.0001$) calculated by Student's t test between strains at the same day.

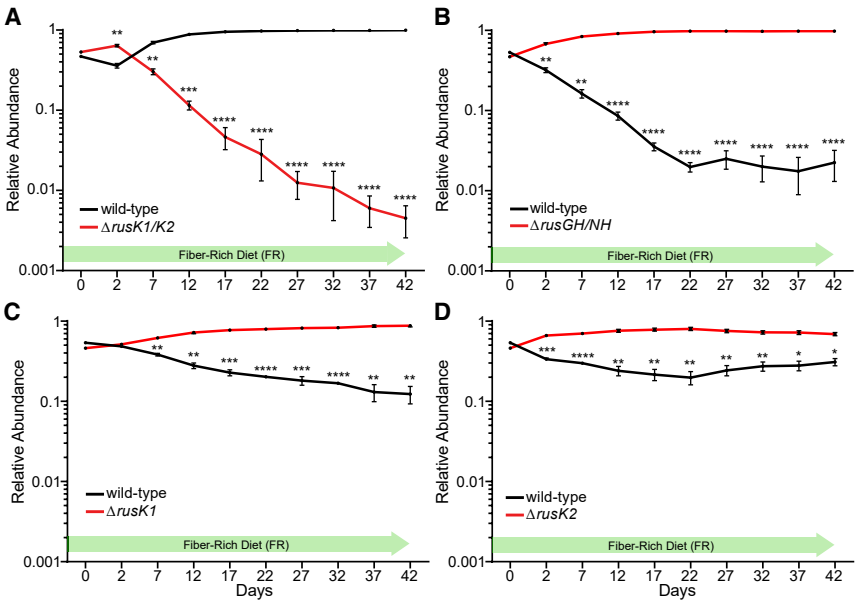

Figure 3. Ribokinases Are Required for Competitive Advantage *In Vivo*

In vivo competition between wild-type *Bt* (black line) and individual mutant strains indicated (red line) in 6- to 8-week-old, germfree Swiss-Webster mice fed the FR diet. Relative abundance is displayed as in Figure 2. In all panels, the mean of n = 4 biological replicates ± SEM is shown. Asterisks indicate significant differences (*p < 0.05, **p < 0.01, ***p < 0.001, and ****p < 0.0001) calculated by Student's t test between strains at the same day.

predicted functionality (Figure 1B) and performed additional competitive colonization experiments in FR diet-fed mice. We inoculated each individual mouse group with wild-type *Bt* and one of the following competing strains—Δ*rusK1/2*, Δ*rusC/D*, Δ*rusGH/NH*, Δ*rusT*, or Δ*rusR*—to test the predicted contributions of phosphorylation, outer membrane transport, hydrolase activity, inner membrane transport, and regulation, respectively. Surprisingly, only the Δ*rusK1/K2* strain, which lacks both predicted ribokinases, exhibited a competitive fitness defect similar to that of the full Δ*rus* mutant (Figure 3A). In contrast, the other deletion strains exhibited equal or better competition in comparison with wild type (Figures 3B and S2D–S2F). These results show that the required functions underlying the competitive defect in the Δ*rus* strain are encoded by the *rusK1* or *rusK2* genes, whereas other functions provide no advantage and perhaps a fitness disadvantage on the FR diet. We speculate that the advantages exhibited by the other mutants are a result of not incurring the cost of expressing these proteins in a condition where they do not participate in acquiring nutrients, a phenomenon observed with *Bt* fungal mannan utilization (Cuskin et al., 2015). To test whether only one of the two ribokinases is most important *in vivo*, we repeated the above competition with single Δ*rusK1* and Δ*rusK2* deletion strains. Each of these single-kinase mutants also competed better than wild type, suggesting functional redundancy in this context (Figures 3C and 3D). Genetic complementation of the Δ*rusK1/K2* strain restored the competitive ability of the defective mutant strain, allowing equal competition against wild type (Figure S2G). Finally, variations in competitive behavior were not attributable to significant differences in *rus* expression in wild-type *Bt* for any of the *in vivo* competitions (Figure S2H).

Rus Functions Are Required for Sensing and Utilization of RNA, Nucleosides, and Other Nutrients *In Vitro*

The results described above indicate a diet-specific advantage for *Bt* strains containing *rus*-encoded ribokinases. To further define this system's function, we tested our panel of deletion mutants in a variety of growth conditions, including free ribose, nucleosides, RNA, and other sources of ribose. Consistent with *in vivo* data, a mutant lacking both *rusK1* and *rusK2* could not grow on free ribose (Figure 4A). Arguing against purely redundant functions, the mutant lacking just *rusK2* displayed a complete loss of growth phenotype, whereas a mutant lacking only *rusK1* reproducibly displayed a substantial growth lag but eventually grew with a slightly slower rate than did wild type (Figures 4B and 4C). The delayed growth of this mutant could be due to a genetic suppressor mutation because cells that eventually grew were able to grow quickly on ribose after being isolated and passaged in rich media (Figure S3A). Deletion of the flanking gene *rusR*, a candidate transcriptional regulator, resulted in an inability to grow on ribose. This suggested that although it is not transcriptionally activated in response to ribose, it plays an essential role in ribose catabolism (Figure 4D). In comparison with wild type, the Δ*rusT* strain exhibited increased lag, slower growth rate, and lower overall growth (Figure 4E). Unlike the Δ*rusK1* mutant, this mutant did not exhibit increased growth after passage (data not shown), suggesting that suppressor mutations are not involved but that perhaps a lower-affinity sugar permease imports ribose less efficiently. All of the other single- or double-deletion mutants (Δ*rusC*, Δ*rusD*, Δ*rusC/D*, Δ*rusGH,* Δ*rusNH*, and Δ*rusGH/NH*), as opposed to wild-type *Bt*, exhibited no measurable differences in growth on ribose (Figures S3B–S3G; Table S1). The growth defects associated with Δ*rus*K1/K2 and Δ*rusR* were fully repaired by a single, complementing copy of each gene in *trans* (Figure 4F; *rusT* was not attempted).

Because of their larger and more complex structure, we hypothesized that utilization of covalently linked ribose sources would require the additional *rus*-encoded outer membrane transport and hydrolase functions. To test this, we assayed growth of our *rus* mutants and wild-type *Bt* on nucleosides and RNA. Wild-type *Bt* displayed no or poor growth on all nucleosides tested and on RNA (Figures S3H and S3I; Table S1). We hypothesized that free ribose could be required for activating transcription of the *rus* locus and thus generating proteins necessary for catabolism of these substrates. We determined a concentration (0.5 mg/mL) at which ribose elicited strong *rus* expression but little measurable growth on the basis of absorption measurement (Figures S3J and S3K). We then re-evaluated the ability of wild-type *Bt* to grow on nucleosides and observed considerably higher levels of growth on pyrimidine nucleosides

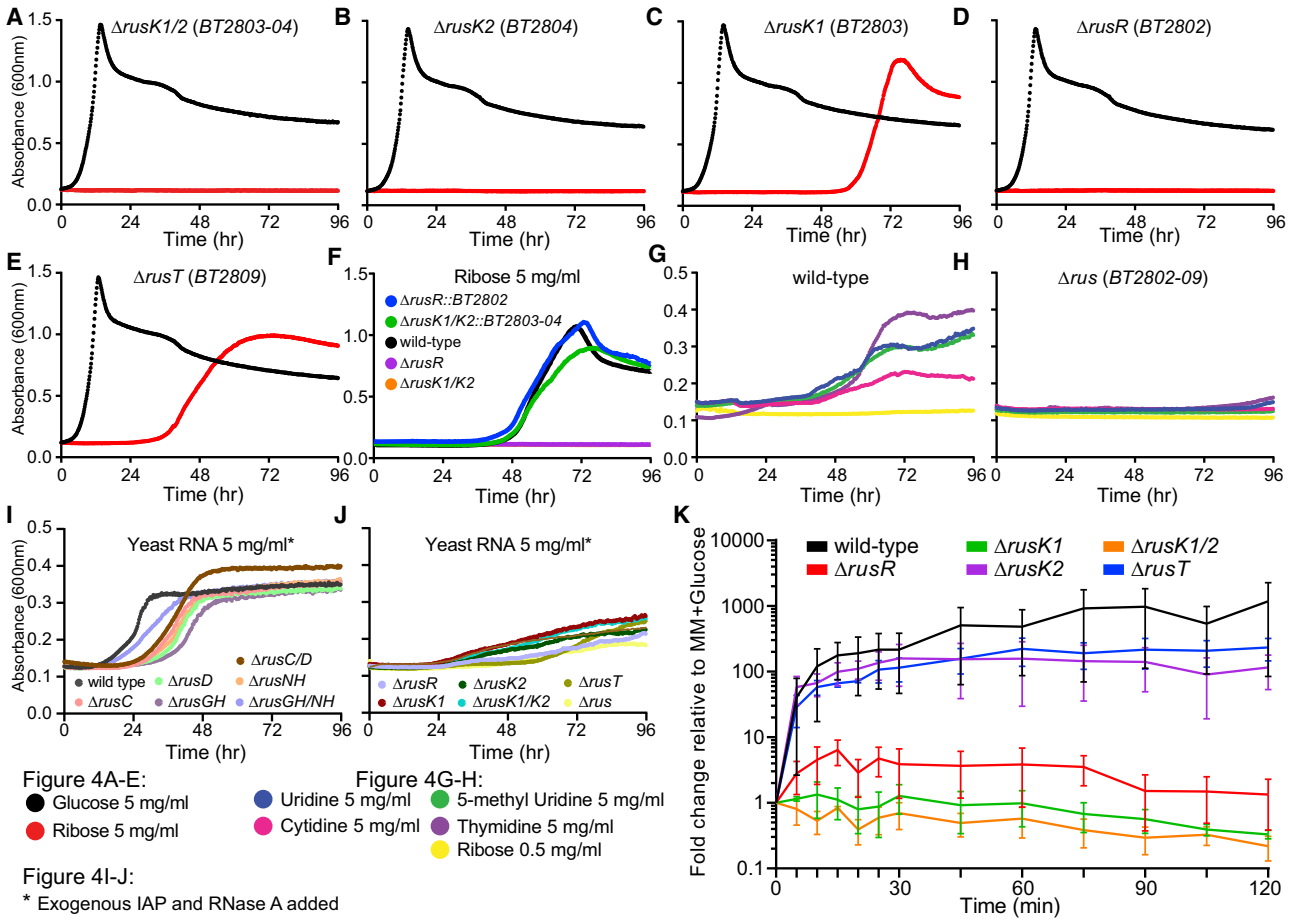

Figure 4. The *Bt rus* PUL Encodes Functions Required for Growth and Transcript Activation on Ribose-Containing Nutrients

(A–E) Growth curves of the individual *rus* deletion strains indicated (red lines); growth on glucose (black line) is a control. (A) *ΔrusK1/2* (*BT2803 and BT2804*), (B) *ΔrusK2* (*BT2804*), (C) *ΔrusK1* (*BT2803*), (D) *ΔrusR* (*BT2802*), and (E) *ΔrusT* (*BT2809*).

(F) Growth of genetically complemented Δ*rusR* (blue line) and Δ*rusK1/K2* (green line) on ribose shows restored growth in comparison with wild-type (black line) and corresponding deletions (purple and orange lines).

(G and H) Wild-type (G) or Δ*rus* (H) growth on nucleosides in the presence of 0.5 mg/mL ribose (yellow line is medium with only 0.5 mg/mL ribose). Legend in bottom right shows substrates tested.

(I and J) Wild-type *Bt* and *rus* deletion strains grown in MM, plus 5 mg/mL yeast RNA with RNase A and IAP. Mutants with similar growth phenotypes as wild-type (I) are compared with mutants with reductions in growth (J).

(K) *Bt rusC* transcript activation measured by qRT-PCR after mid-log phase cells grown in MM-glucose were washed in carbon-free medium and transferred to MM-ribose.

For all strains, samples were taken every 5 min for 30 min after exposure and then every 15 min until 120 min after exposure. Strains are color coded according to the key provided. Data shown are the mean of n = 3 separate experiments ± SEM.

(Figure 4G). Growth was comparatively poor in comparison with growth on ribose; increased growth was not observed by doubling nucleoside concentrations, suggesting that something else related to nucleoside catabolism limits growth (Figure S3L).

Importantly, growth on nucleosides was eliminated in mutants lacking the full *rus* locus (Figure 4H), either or both ribokinases, the candidate regulator (*rusR*), or the putative transporter (*rusT*) (Figures S3M–S3Q). Growth on RNA was not observed after addition of ribose, suggesting that *Bt* does not produce sufficient extracellular RNase and phosphatase enzymes to liberate nucleosides. Therefore, we tested whether exogenously added RNase A and intestinal alkaline phosphatase (IAP), both present in the gut from pancreatic secretions (RNase) or the enterocyte brush boarder (IAP), could enhance growth on RNA at physiologically relevant concentrations (McConnell et al., 2009; Weickmann et al., 1984). These enzymes supported appreciably more growth on RNA (Figure 4I), not attributable to *Bt*'s growth on the exogenous enzymes themselves (Figure S3R). As with individual nucleosides, reductions or eliminations in growth on enzyme-degraded RNA were observed in mutants lacking the entire *rus* locus, *rusK1*, *rusK2*, *rusK1/K2*, *rusT*, and *rusR* (Figure 4J). Further, mutants lacking predicted transport and hydrolytic functions grew similarly to wild type on both nucleosides and degraded RNA (Figures 4 and S3S–S3X). In addition, we determined that *Bt* utilizes deoxyribose and lyxose, as well as ADP-ribose, UDP-galactose, and UDP-α-glucose. All of these

required the presence of a low amount of ribose and the *rus* locus, whereas 21 other substrates did not support *Bt* growth under any conditions tested (Table S1).

On the basis of our mutant growth phenotypes, we sought to determine whether the genes required for ribose growth were also required for activating expression of *rus.* We examined the kinetics of *rus* transcriptional responses when *Bt* was exposed to ribose, an assay that allows us to measure response independent of ability to grow on ribose. Interestingly, the Δ*rusK2* strain, which cannot grow on ribose, generated transcript at a rate similar to that of wild type up to 2 h (Figure 4K). In contrast, the Δ*rusK1* mutant, which exhibited an extensive lag before growth on ribose, was unable to quickly generate transcript within 2 h but eventually achieved near wild-type *rus* expression once it actively grew on ribose because of its suspected suppressor (Figures 4K and S4D). As expected, the Δ*rusK1/K2* double mutant did not generate transcript. The Δ*rusR* mutant achieved partial (∼10%) activation, supporting the hypothesis that RusR is a positive-acting regulator. The Δ*rusT* strain only has a slight defect, suggesting that another, non-specific permease can transport ribose. We also measured *rus* expression dynamics in our Δ*rusC* and Δ*rusD* strains but failed to detect any differences to wild type, consistent with the lack of their requirement for ribose growth (Figure S4E). Finally, the nucleosides uridine and inosine did not serve as *rus*-inducing molecules in wild-type *Bt* (Figure S4F).

Non Rus-Encoded Functions Are Required for Nucleoside Utilization

The lack of a requirement for the *rus* hydrolase functions in nucleoside catabolism is noteworthy, given that we confirmed through biochemical experiments with recombinant enzyme that RusNH is a genuine, albeit weak, nucleoside hydrolase (Table S2A) and that RusGH can cleave *p*-nitrophenyl-β-D-riboside (Tables S2B and S2C). The lack of a phenotype associated with loss of RusNH suggested that other functions in *Bt* are responsible for cleavage of free pyrimidine nucleosides or those liberated from RNA. To identify alternative enzymes, we searched the *Bt* genome for functions from known nucleoside scavenging systems (NSSs) and identified several candidates. We made deletions of four genes predicted to encode nucleoside phosphorylase (*BT1881* and *BT4554*), uridine kinase (*BT0184*), and nucleoside permease (*BT4330*) activities and tested growth of these mutants on pyrimidine nucleosides (Figures 5A–5C and S4A). One strain (Δ*BT4554*) displayed loss of growth on all nucleosides tested, suggesting that it encodes an essential enzyme for cleaving nucleosides and might work upstream of the *rus* functions, which are also required. The Δ*BT4330* mutant exhibited reductions in growth on uridine, cytidine, and 5-methyl uridine (Figures 5A–5C) and only a slight defect on thymidine (Figure S4A). The Δ*BT0184* mutant displayed enhanced growth that began quicker than wild-type growth and reached a higher total growth level on all nucleosides, except on thymidine. This phenotype could be due to its role in 5′-phosphorylating scavenged nucleosides and shunting them toward anabolic pathways, such that its loss favors catabolism. Like the wild type, Δ*BT1881* did not display any detectable growth defects, suggesting that the product of this gene is not essential for pyrimidine catabolism.

To understand how these NSS functions could affect gut colonization, we tested the Δ*BT4554* mutant in our *in vivo* competition assay. In mice fed the FR diet, this mutant exhibited a similar 2–3 order of magnitude defect that closely resembled those of the Δ*rus* and Δ*rusK1/K2* mutant strains (Figure 5D). This finding helps connect the role of *rus* functions, which in all of the conditions assayed were ubiquitously expressed *in vivo*, and the FR-diet-specific fitness advantage experienced by wild-type *Bt in vivo*. We cannot definitively determine that nucleosides are the *in-vivo*-scavenged nutrients that drive this competitive advantage. However, (1) similarity of the Δ*rus*, Δ*rusK1/K2*, and Δ*BT4554* phenotypes and (2) the dependence on both a small amount of ribose (i.e., to induce *rus*) and a functional *rus* system for *in vitro* growth on nucleosides via BT4554 support a model in which ribose-induced Rus kinases are essential for the *in vivo* scavenging of nucleosides processed by BT4554. Although growth on nucleosides in some NSS mutants was reduced or eliminated, this phenotype did not extend to growth on RNA or ribose because the mutant strains exhibited levels of growth similar to those of the wild type (Figures S4B and S4C). This suggests that, although Rus functions are required for the utilization of RNA, the NSS functions interrogated here are not individually essential for catabolism of RNA-derived nucleosides or oligos.

Rus Kinases Are Active toward Ribose- and Nucleoside-Derived Ribose-1-Phosphate

To scrutinize the activities of the *rus*-encoded kinases in detail, we produced recombinant forms and performed *in vitro* phosphorylation assays against pentose sugars and other monosaccharides (*E. coli* RbsK was a positive control). RusK2 has a preferred specificity toward ribose and deoxyribose while exhibiting weaker activity on arabinose and xylose (Table S2D). RusK1 displayed nearly 10-fold weaker activity on ribose and deoxyribose than did RusK2 and weak activity toward other sugars tested (Table S2D). The initial assay used to measure activity from RusK1 and RusK2 did not determine positional phosphorylation specificity. We hypothesized that an important difference in these kinases might be their positional phosphorylation at either the 1 or 5 carbon of ribose. When RusK1 and RusK2 enzymes were incubated with ribose and analyzed by LC-MS/MS, both generated ribose-5-phosphate (R5P) as the major detectable product (Figure 5E). We did not detect formation of ribose-1-phosphate (R1P) from ribose despite being able to reliably distinguish this compound as a standard (Table S2E). We next performed reactions with R1P as the substrate to test whether this product, which we expect to be generated by BT4554 phosphorolysis of nucleosides, could be a substrate for the Rus kinases. Interestingly, our results show that ribose-1,5-bisphosphate (PRibP) is generated from R1P by both RusK1 and RusK2 (Figure 5F). In addition, RusK2 could generate a product with the same predicted mass as PRibP when given R5P as a substrate, even though RusK2 did not form R1P from ribose (Figure 5F). The mechanism involved in generating PRibP, or ribokinases capable of phosphorylation in the 1 position, has not yet been identified in eubacteria. Rather, generation of PRibP by a different family of kinases has been described in archaea and plants as part of the RuBISCO pathway (Hove-Jensen et al., 2018). Our results help connect the function of Rus-encoded kinases with

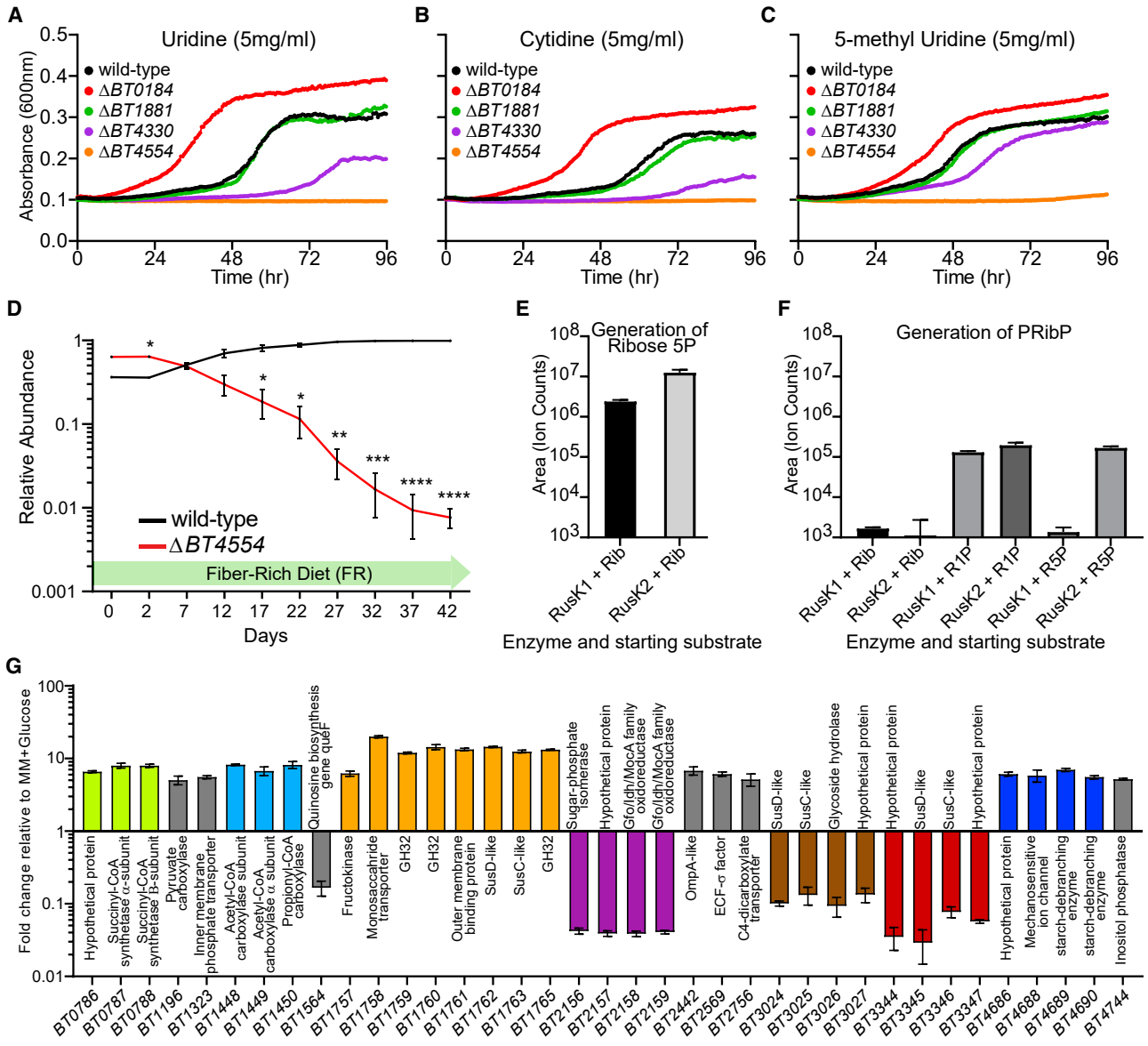

Figure 5. Requirements for *Bt* Nucleoside-Scavenging Systems, Positional Phosphorylation by Ribokinases, and Global Responses to Ribose

(A–C) Growth curves of nucleoside-scavenging gene-deletion strains (colored according to key) versus wild-type *Bt* (black) on uridine (A), cytidine (B), or 5-methyl uridine (C).

(D) *In vivo* competition between wild-type *Bt* (black) and Δ*BT4554* strains (red) shows the relative abundance on the FR diet with mean ± SEM of n = 4 biological replicates.

(E and F) Positional ribose phosphorylation by RusK1 or RusK2 measured by LC-MS-MS for ribose 5-phosphate (E) or ribose-1,5-bisphosphate (F); for each bar the mean of n = 3 biological replicates ± SD is shown. The y axis minimum of 10^3 was determined from negative control reactions that included control enzyme or buffer only (Table S2E). Detection of PRibP was based on a PRPP standard fragmenting into the major species of PRibP of the exact expected mass.

(G) RNA-seq-based global transcriptomic responses in *Bt* grown on MM-ribose compared with MM-glucose.

Same bar color indicates genes in the same locus. Genes with gray bars are not physically linked in the genome. For each bar, the mean of n = 3 replicates is shown ± SD. In (E), asterisks indicate significant differences (*p < 0.05, **p < 0.01, ***p < 0.001, and ****p < 0.0001) calculated by Student's t test.

BT4554-mediated nucleoside scavenging via generation of intermediate PRibP. The route that PRibP takes after it is produced is still uncertain because *Bt* lacks a clear homolog of the *E. coli* ribose 1,5-bisphosphokinase (*phnN*) that consumes PRibP to generate phosphoribosyl pyrophosphate (PRPP), which can be used in nucleic acid synthesis or catabolically via the pentose-phosphate pathway. Nevertheless, our data suggest that the similar *in vivo* defects associated with loss of either RusK1/K2 or BT4554 are due to the requirement of both systems for utilization of exogenous nucleosides

Global Responses to Ribose Catabolism

We hypothesized that growth on ribose could affect expression of a global regulon. To test this, we performed RNA-sequencing (RNA-seq)-based whole-genome transcriptional profiling on wild-type *Bt* grown on ribose or glucose. Indeed, the data revealed a global response in which 81 genes were differentially expressed on the basis of the parameters and thresholds used. Many of the genes (46%) belong to other PULs or metabolic pathways (Table S3). Notable changes included upregulation of a previously defined PUL for fructose and β2,6-linked fructan metabolism (*BT1757–1765*; average 15-fold upregulation), which interestingly liberates fructose that initiates the pentose phosphate pathway (PPP) (Sonnenburg et al., 2010) and suppresses *rus* expression (Figure S1A). At the same time, two other PULs of unknown specificity (*BT3024–3027* and *BT3344–3347*) were repressed. Further, several genes encoding tricarboxylic acid (TCA) cycle enzymes leading to generation of succinate and propionate, of which *Bt* has a partial pathway (Pan and Imlay, 2001), were upregulated. In contrast, genes predicted to participate in sugar-phosphate isomerization and metabolism were strongly repressed (*BT2156–2159*; average of 24-fold) (Figure 5G). An experiment to test whether cross-regulation between ribose metabolism and the fructan PUL contributes to the FR-diet-specific competitive defect failed to support this model (Figures S4G and S4H).

An Enzyme-Diversified Family of Rus Systems Exists throughout the Bacteroidetes

The data described above support the idea that the *Bt rus* PUL is necessary, but not always sufficient, for metabolizing ribose and nucleosides. Because it is strongly activated in response to the simple sugar ribose and not an oligosaccharide cue, *rus* is relatively unique and only the second PUL after the *Bt* fructan PUL shown to be activated in response to a monosaccharide (Sonnenburg et al., 2010). The architecture of this system suggests that it is equipped to liberate ribose from additional unknown sources via its hydrolases. Therefore, we hypothesized that *rus*-like systems could be found in other gut isolates and perhaps more broadly across the Bacteroidetes. To test this, we measured the growth ability of 354 different human and animal gut Bacteroidetes in MM-ribose, revealing that ribose utilization is widely but variably present in different species (Figures 6A and S5A; Table S4). To determine whether sequenced representatives of the species and strains that grow on ribose contain a homolog of the experimentally validated *Bt rus*, we used comparative genomics to search for homologs of this PUL within these gut isolates. This revealed that all of the sequenced strains that grow on ribose possess a candidate *rus*-like PUL, whereas none of the strains unable to grow on ribose have a homologous gene cluster. Interestingly, our analysis revealed very similar homologs of some *rus* genes in sequenced gut isolates (e.g., *Prevotella*) beyond those present in our initial survey. When we expanded the search to include Bacteroidetes isolates found in other body sites and in the environment, we detected *rus*-like systems across the phylum and found that systems in the genus *Bacteroides* were most similar to the prototype from *Bt*. Remarkably, we identified a total of 70 different *rus* configurations, ranging from simple two-gene units (permease and kinase) to *rus* PULs containing as many as 36 genes (Figures 6B and S5B). For almost all *rus*-like systems, the following genes were present: *rusC* and *rusD*, an upstream *rusR* (or to a lesser extent different regulator types), either one or two *rusK* genes, and a *rusT* homolog. Perhaps most intriguingly, the predicted enzymes found in different *rus*-like systems are exceptionally variable; there are at least 22 different predicted glycoside hydrolase families, ADP-ribosylglycohydrolases, carbohydrate esterases, and nucleoside hydrolases, among others. This plethora of enzymatic potential encoded in *rus* homologs across the Bacteroidetes suggests that individual species or strains target different ribose-containing nutrients. To further connect these predicted *rus*-like systems with ribose utilization, we probed the transcriptional response of eight different systems during growth on MM-ribose and found that all strains tested exhibited ~100- to 1,000-fold upregulation in relation to an MM-glucose reference (Figure 6C).

DISCUSSION

Diet affects the gut microbiota in many ways, and members of the prominent Bacteroidetes phylum have developed sophisticated strategies to liberate sugars from very complex dietary fiber polysaccharides, such as pectins (Luis et al., 2018; Ndeh et al., 2017). Such abilities equip these bacteria to compete for dietary and endogenous nutrients to sustain their populations. Diet-, microbiome-, and host-derived RNA, nucleosides, cofactors, and other sources of ribose have been largely unexplored as potential nutrients scavenged by members of the gut microbiota. Our findings demonstrate that *Bt* utilizes free and covalently linked sources of ribose and that this metabolic capability contributes to competitive fitness *in vivo* in a diet-dependent fashion—most likely through a more complicated metabolic mechanism that interconnects ribose sensing and nucleoside scavenging (Figure 7). It is also clear from comparative genomics that the ability to access ribose from diverse sources extends across the Bacteroidetes phylum and is present in many animal gut, oral, and environmental isolates.

Although we have not yet uncovered a more complex ribose-containing polymer requiring Rus transport and hydrolase functions, a key aspect of our ribose-utilization model is that Rus-encoded kinases are required for growth on free and RNA-derived nucleosides, the latter only after RNase and IAP degradation (Figure 7). In light of this pathway for nucleoside assimilation, the roles of periplasmic RusNH and cell-surface RusGH remain enigmatic. Given the weak activities of these enzymes toward the substrates tested, it is probable that they are optimized to cleave substrates that we have not yet been able to test and that are the bona fide nutrient targets of the *Bt* Rus system. At least for the pyrimidine nucleosides tested *in vitro*, the BT4554 phosphorylase, which generates a cleaved base plus R1P, is the primary component required. A novel aspect of the model we have determined for *Bt* is that Rus-encoded ribokinases are required for conversion of R1P to PRibP, and this conversion requires ribose induction of Rus to activate production of the ribokinases. This interconnection could stem from the dual function of the ribokinases, phosphorylating both ribose to R5P and R1P to PRibP. On the basis of our growth and positional phosphorylation data, it is unlikely that R5P is being shunted directly into catabolism as canonically represented in KEGG

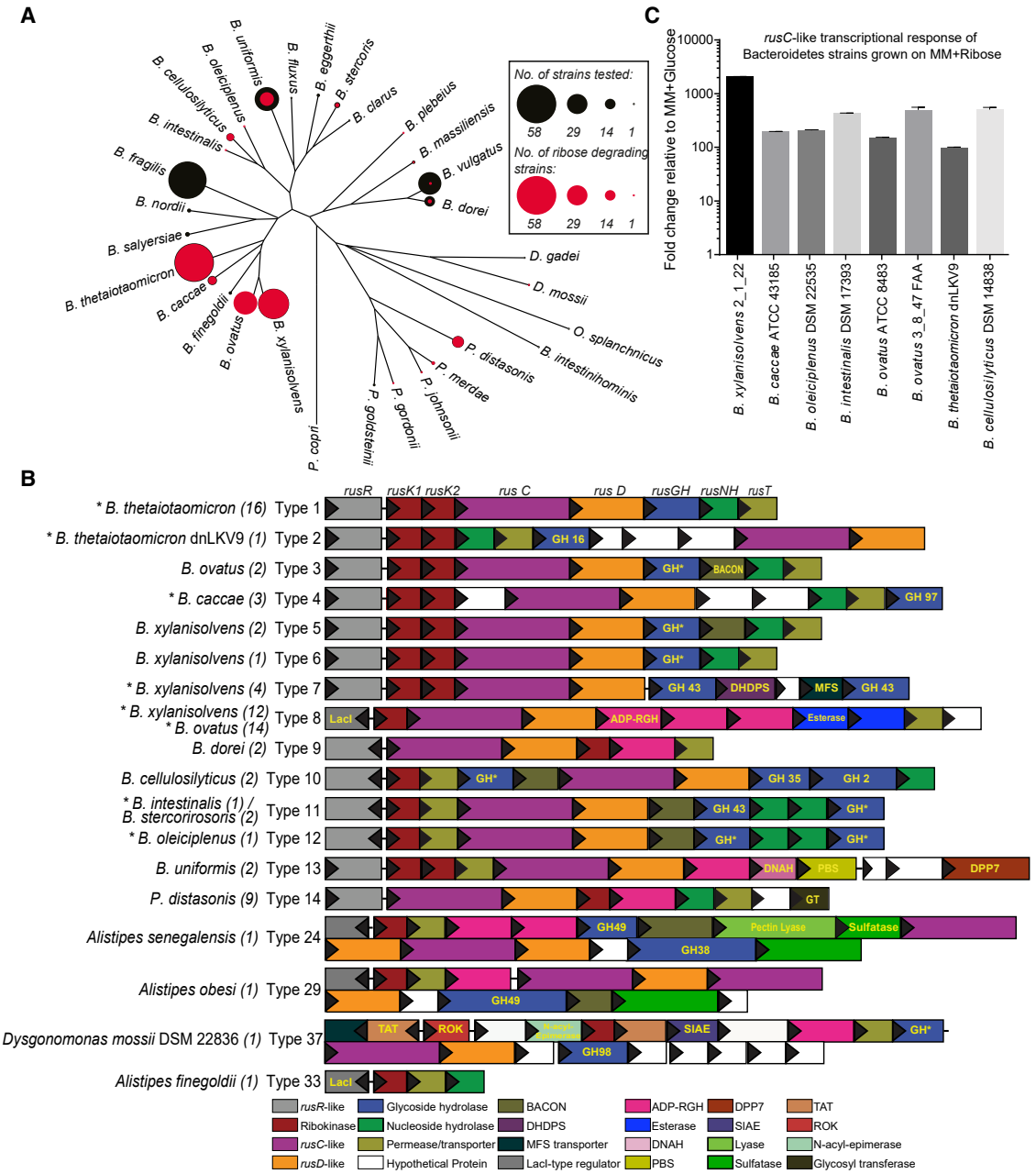

Figure 6. Ribose Utilization Is Present across the Bacteroidetes Phylum with Many Configurations of Corresponding *rus* PULs

(A) Genus-level phylogeny constructed from sequenced isolates shows the presence of ribose utilization. Outer black circles are sized to represent the number of strains tested for each species. Inner red circles indicate the number of tested strains that grow on ribose.

(B) Comparisons of several variants of *rus* PULs throughout the Bacteroidetes. Identical background color indicates the same predicted functions, which are defined according to the key. The number of sequenced isolates that harbor each PUL type is listed adjacent to each schematic, and each variant is assigned an arbitrary type number detailed in Table S5. Asterisks next to the organism name indicate that the PUL type shown is upregulated by ribose as the sole carbon source in at least one strain tested. Genes are sized to scale, and all species represented here are human gut isolates. A broader representation of *rus* diversity is shown in Figure S5 and includes PULs from environmental and oral Bacteroidetes. Abbreviations not previously defined in the text are as follows: GH*, Glycoside hydrolase of unknown family or function; BACON, Bacteroidetes-associated carbohydrate-binding often N-terminal domain; DHDPS, dihydrodipicolinate synthase; LacI, predicted lacI-type transcriptional regulator; MFS, major-facilitator superfamily of transporters; ADP-RGH, ADP-ribosyl glycoside hydrolase; DNAH, DNA helicase; PBS, polysaccharide biosynthesis and export of O-antigen and techoic acids; DPP7, dipeptidyl-peptidase 7 (serine peptidase); GT, glycosyl transferase.

(C) Fold change of *rusC*-like transcript from the indicated species and/or strain shows that several additional *rus* PULs are activated during growth on ribose as compared with glucose. Error bars show the SEM of n = 3 biological replicates.

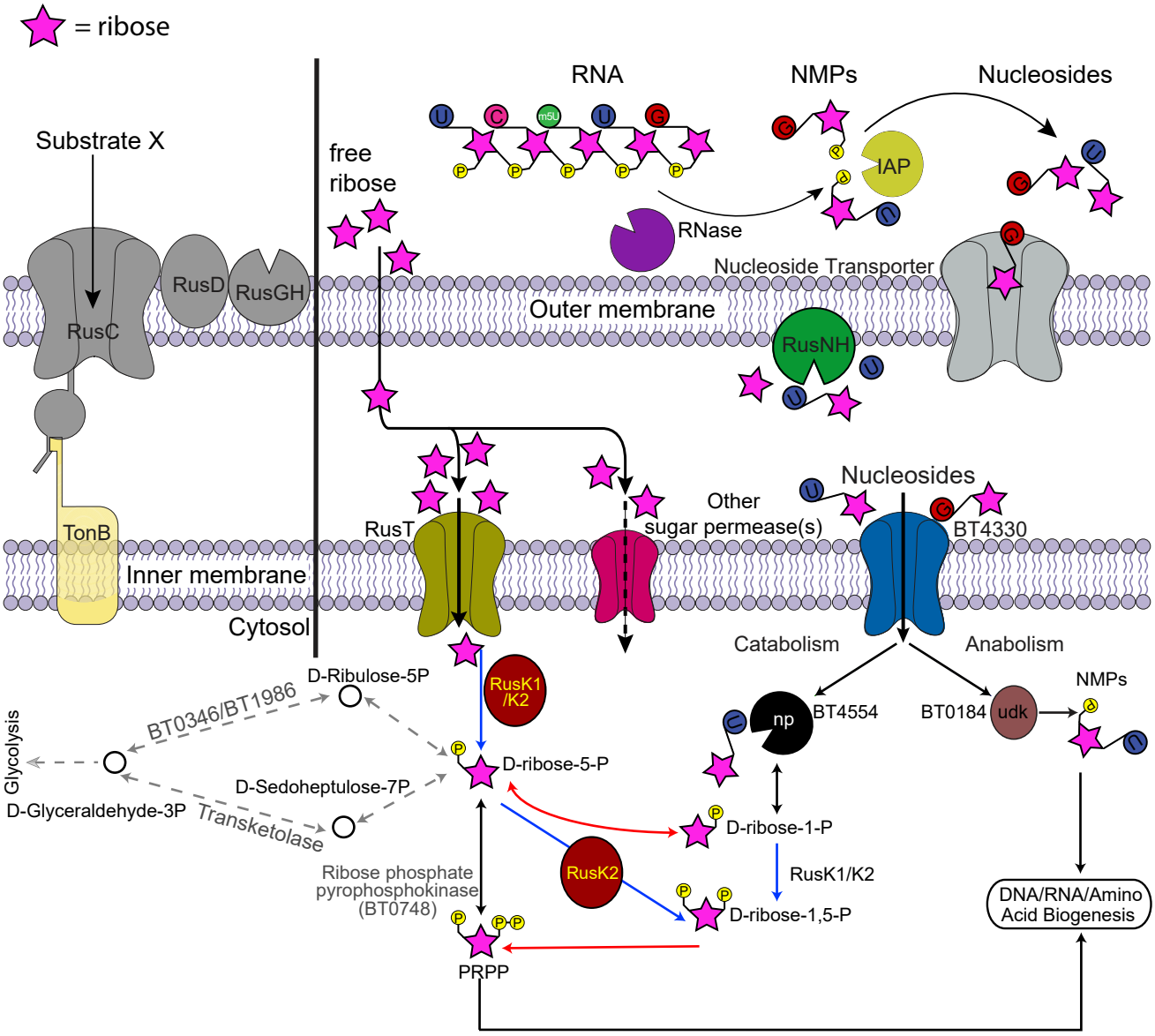

Figure 7. Model of Ribose Utilization by *Bt* and Connection to Nucleoside Scavenging

The model shown represents a proposed mechanism of ribose and nucleoside metabolism via *rus*-encoded functions and nucleoside-scavenging systems based on the data in this study and predicted KEGG metabolic maps. Ribose is depicted as a pink star, phosphate groups are represented as yellow circles, and nucleoside bases are shown as colored circles (blue, uridine; green, 5-methyl uridine; dark pink, cytidine; red, guanosine). Some cellular locations of protein products were experimentally determined (e.g., Figure S6 for localization data for RusGH and RusNH). Proteins for which no functional requirement could be assigned (RusC, RusD, and RusGH) are shaded in gray. Abbreviations are as follows: IAP, intestinal alkaline phosphatase; RusNH, *rus*-encoded nucleoside hydrolase; RusK1/K2, ribokinases; np, nucleoside phosphorylase; uridine kinase, udk. Our cytosolic metabolic model depicts our interpretation of the PPP of *Bt* according to our results. Dashed arrows with a red "x" indicate that homologs of the enzymes normally catalyzing these steps are not detectable by homology searching in *Bt*. Black arrows are PPP steps that most likely occur in *Bt*, and we have results indicating the importance of BT0184, BT4330, and BT4554 in nucleoside catabolism.

maps of the PPP. This is largely based on the observation that either Rus kinase can generate R5P, so if direct assimilatory pathways exist through D-ribulose-5-P or D-sedoheptulose-7-P, then both single-kinase mutants should grow normally because they would be redundant in this function. Rather, PRibP, which is generated from R1P or R5P and whose ultimate path or paths are uncertain, is more likely the relevant molecule being generated for use in catabolism. The lack of a detectable phosphopentomutase in *Bt* that isomerizes R5P to R1P (having only a phosphoglucomutase, BT1548) could have driven the evolution of co-dependence on the ribokinases and nucleoside phosphorylase (BT4554) to generate PRibP. Although the full catabolic pathway for PRibP in *Bt* is still unclear, our findings hold important implications for how predicted metabolic maps could be

incomplete in some instances and should be interpreted with caution. By investigating this pathway more deeply, we demonstrate previously undescribed bacterial ATP-dependent ribokinases able to generate PRibP from R1P.

Similar to only one other previously characterized *Bacteroides* PUL for fructan utilization (Sonnenburg et al., 2010), the *rus* PUL is activated in response to a monosaccharide (fructose and ribose for the respective systems) (Figure 1C) and also contains a dedicated permease and kinase, revealing that these two systems are similarly patterned around a core monosaccharide utilization pathway. Although the activation signal for *rus* is derived from extracellular ribose, we are unable to conclude the exact phosphorylation status of the ribose that activates expression. Our results show that the kinases and the putative regulator RusR are required for generation of transcript. Often, the enzyme content encoded in Bacteroidetes PULs provides a window into the nutrient linkages that any given system has evolved to target (Cuskin et al., 2015; Larsbrink et al., 2014; Temple et al., 2017). Ribose is present in many diverse sources with different linkages, including RNA and nucleosides, bacterial capsules, cofactors such as NAD, cellular modification such as (poly) ADP-ribose, and more exotic molecules such as microcins (Duquesne et al., 2007). The breadth of enzymatic diversity emphasized by the presence of at least 22 different glycoside hydrolase families plus others and 70 different configurations of ribose-utilization systems across the phylum supports a hypothesis whereby species have adapted to liberate ribose from different and diverse sources. We initially hypothesized that the nutrient mediating the competitive advantage *in vivo* for *Bt rus* would be endogenous nucleosides or RNA from bacteria or host cells in a FF diet. However, our results suggest that in the FR diet, nucleosides are the nutrients targeted by the combined actions of BT4554 and the *rus* kinases. Although pyrimidine nucleoside addition to water in mice fed the FF diet did not reveal a competitive defect, it is possible that purine nucleosides, which were not tested because of low solubility, could be present in the FR diet and exert this effect.

The results described here highlight how survival of bacteria in the human gut and other ecosystems has driven adaptations to sense and scavenge the ubiquitous sugar ribose. Because enterohemorrhagic *E. coli* (EHEC) and other pathogenic *E. coli* preferentially utilize ribose *in vivo* (Fabich et al., 2008; Martinez-Jéhanne et al., 2009) or upregulate genes for the catabolism of this nutrient in the environment (Bufe et al., 2019), these substrates could represent unexplored nutrient niches competed for by commensal and pathogenic microorganisms and could therefore help mediate colonization resistance against pathogens. The evolution of diverse enzyme functions throughout the Bacteroidetes could be analogous to a molecular "Swiss Army knife," in which the core function is utilization of ribose, but the various blades and other implements represent the enzymes equipping the system to sense, import, or harvest ribose from diverse sources. This molecular adaptability is particularly important in the context of the nutrient niche hypothesis of gut bacterial survival. Although some nutrients could be scarce in comparison with abundant dietary fiber polysaccharides, competition for these lower-abundance nutrients could be less intense, and organisms capable of accessing them could thereby occupy a stable niche. Although a number of gut bacteria, including pathogens, are capable of utilizing free ribose, the *Bacteroides* could have developed a more sophisticated ability to scavenge multiple sources by cleaving it from covalently linked forms. From this perspective, understanding the struggle to access this "simple" sugar could reveal additional layers underpinning the interplay between native gut mutualists and invading pathogens.

STAR★METHODS

Detailed methods are provided in the online version of this paper and include the following:

- KEY RESOURCES TABLE
- LEAD CONTACT AND MATERIALS AVAILABILITY
- EXPERIMENTAL MODEL AND SUBJECT DETAILS
  - Gnotobiotic Mouse Experiments
  - Bacterial Strains, Culturing Conditions, and Molecular Genetics
- METHOD DETAILS
  - Genetic Manipulation and Recombinant Protein Purification in *E. coli*
  - Measurements of Transcriptional Responses by qPCR
  - Antibody Production, Western Blotting and Immunofluorescent Microscopy
  - Functional Annotation and Comparative Genomics of *rus* PULs across Bacteroidetes Genomes
  - RNaseq Analysis
  - Enzyme Assays
  - Determination of Free and Acid Hydrolysable Monosaccharide Content in Diets and Cecal Contents Using GC/MS
  - LC/MS/MS Determination of Positional Ribose Phosphorylation by *rus* Ribokinases
- QUANTIFICATION AND STATISTICAL ANALYSIS
- DATA AND CODE AVAILABILITY

SUPPLEMENTAL INFORMATION

Supplemental Information can be found online at https://doi.org/10.1016/j.chom.2019.11.009.

ACKNOWLEDGMENTS

R.W.G. was supported by the NIH Molecular Mechanisms in Microbial Pathogenesis training grant (T32AI007528). This work was supported by NIH grant number AI128120. A.S.L. is supported by the Marie Skłodowska-Curie Individual Fellowship (grant no. 748336). Metabolomics studies performed at the University of Michigan were supported by NIH grant DK097153. We would like to thank the Germ-Free Mouse Facility at the University of Michigan for expert assistance with *in vivo* experiments. We would also like to thank N.M. Koropatkin and R.M. Pollet of the University of Michigan Department of Microbiology and Immunology for helping formulate ideas for enzyme purification and assay development, as well as members of the Martens lab for fruitful discussion of the results.

AUTHOR CONTRIBUTIONS

R.W.G. and E.C.M. designed the experiments. R.W.G. conducted the bulk of experiments and performed data analysis. Y.T. and A.I.T. performed GC-MS analysis, and B.R.H. provided helpful insight. P.S. and C.A.L. conducted LC-MS-MS experiments and analysis. A.S.L. assisted in enzyme purification.

N.A.P. performed the growth assays on ribose for the 354 *Bacteroides* isolates. R.W.G. and E.C.M. wrote the paper.

DECLARATION OF INTERESTS

The authors declare no competing interests.

Received: March 12, 2019
Revised: October 3, 2019
Accepted: November 18, 2019
Published: December 31, 2019

REFERENCES

Bjursell, M.K., Martens, E.C., and Gordon, J.I. (2006). Functional genomic and metabolic studies of the adaptations of a prominent adult human gut symbiont, Bacteroides thetaiotaomicron, to the suckling period. J. Biol. Chem. *281*, 36269–36279.

Briliūtė, J., Urbanowicz, P.A., Luis, A.S., Baslé, A., Paterson, N., Rebello, O., Hendel, J., Ndeh, D.A., Lowe, E.C., Martens, E.C., et al. (2019). Complex N-glycan breakdown by gut Bacteroides involves an extensive enzymatic apparatus encoded by multiple co-regulated genetic loci. Nat. Microbiol. *4*, 1571–1581.

Bufe, T., Hennig, A., Klumpp, J., Weiss, A., Nieselt, K., and Schmidt, H. (2019). Differential transcriptome analysis of enterohemorrhagic Escherichia coli strains reveals differences in response to plant-derived compounds. BMC Microbiol. *19*, 212.

Cameron, E.A., Kwiatkowski, K.J., Lee, B.H., Hamaker, B.R., Koropatkin, N.M., and Martens, E.C. (2014). Multifunctional nutrient-binding proteins adapt human symbiotic bacteria for glycan competition in the gut by separately promoting enhanced sensing and catalysis. MBio *5*, e01441-14.

Chuvikovsky, D.V., Esipov, R.S., Skoblov, Y.S., Chupova, L.A., Muravyova, T.I., Miroshnikov, A.I., Lapinjoki, S., and Mikhailopulo, I.A. (2006). Ribokinase from E. coli: expression, purification, and substrate specificity. Bioorg. Med. Chem. *14*, 6327–6332.

Cuskin, F., Lowe, E.C., Temple, M.J., Zhu, Y., Cameron, E., Pudlo, N.A., Porter, N.T., Urs, K., Thompson, A.J., Cartmell, A., et al. (2015). Human gut Bacteroidetes can utilize yeast mannan through a selfish mechanism. Nature *517*, 165–169.

Datsenko, K.A., and Wanner, B.L. (2000). One-step inactivation of chromosomal genes in Escherichia coli K-12 using PCR products. Proc. Natl. Acad. Sci. USA *97*, 6640–6645.

Desai, M.S., Seekatz, A.M., Koropatkin, N.M., Kamada, N., Hickey, C.A., Wolter, M., Pudlo, N.A., Kitamoto, S., Terrapon, N., Muller, A., et al. (2016). A Dietary Fiber-Deprived Gut Microbiota Degrades the Colonic Mucus Barrier and Enhances Pathogen Susceptibility. Cell *167*, 1339–1353.e21.

Duquesne, S., Petit, V., Peduzzi, J., and Rebuffat, S. (2007). Structural and functional diversity of microcins, gene-encoded antibacterial peptides from enterobacteria. J. Mol. Microbiol. Biotechnol. *13*, 200–209.

Fabich, A.J., Jones, S.A., Chowdhury, F.Z., Cernosek, A., Anderson, A., Smalley, D., McHargue, J.W., Hightower, G.A., Smith, J.T., Autieri, S.M., et al. (2008). Comparison of carbon nutrition for pathogenic and commensal Escherichia coli strains in the mouse intestine. Infect. Immun. *76*, 1143–1152.

Finkel, S.E., and Kolter, R. (2001). DNA as a nutrient: novel role for bacterial competence gene homologs. J. Bacteriol. *183*, 6288–6293.

Glenwright, A.J., Pothula, K.R., Bhamidimarri, S.P., Chorev, D.S., Baslé, A., Firbank, S.J., Zheng, H., Robinson, C.V., Winterhalter, M., Kleinekathöfer, U., et al. (2017). Structural basis for nutrient acquisition by dominant members of the human gut microbiota. Nature *541*, 407–411.

Hammer-Jespersen, K., Munch-Petersen, A., Schwartz, M., and Nygaard, P. (1971). Induction of enzymes involed in the catabolism of deoxyribonucleosides and ribonucleosides in Escherichia coli K 12. Eur. J. Biochem. *19*, 533–538.

Harvey, P.C., Watson, M., Hulme, S., Jones, M.A., Lovell, M., Berchieri, A., Jr., Young, J., Bumstead, N., and Barrow, P. (2011). Salmonella enterica serovar typhimurium colonizing the lumen of the chicken intestine grows slowly and upregulates a unique set of virulence and metabolism genes. Infect. Immun. *79*, 4105–4121.

Hehemann, J.H., Kelly, A.G., Pudlo, N.A., Martens, E.C., and Boraston, A.B. (2012). Bacteria of the human gut microbiome catabolize red seaweed glycans with carbohydrate-active enzyme updates from extrinsic microbes. Proc. Natl. Acad. Sci. USA *109*, 19786–19791.

Holdeman, L.V.E. (1977). Anaerobe laboratory manual (Virginia Ho University).

Hove-Jensen, B., Brodersen, D.E., and Manav, M.C. (2018). The Prodigal Compound: Return of Ribosyl 1,5-Bisphosphate as an Important Player in Metabolism. Microbiol. Mol. Biol. Rev. *83*, e00040-18.

Kim, H.S., Lee, J.H., Lee, W.S., and Bang, W.G. (2006). Genes encoding ribonucleoside hydrolase 1 and 2 from Corynebacterium ammoniagenes. Microbiology *152*, 1169–1177.

Koropatkin, N.M., Martens, E.C., Gordon, J.I., and Smith, T.J. (2008). Starch catabolism by a prominent human gut symbiont is directed by the recognition of amylose helices. Structure *16*, 1105–1115.

Larsbrink, J., Rogers, T.E., Hemsworth, G.R., McKee, L.S., Tauzin, A.S., Spadiut, O., Klinter, S., Pudlo, N.A., Urs, K., Koropatkin, N.M., et al. (2014). A discrete genetic locus confers xyloglucan metabolism in select human gut Bacteroidetes. Nature *506*, 498–502.

Luis, A.S., Briggs, J., Zhang, X., Farnell, B., Ndeh, D., Labourel, A., Baslé, A., Cartmell, A., Terrapon, N., Stott, K., et al. (2018). Dietary pectic glycans are degraded by coordinated enzyme pathways in human colonic Bacteroides. Nat. Microbiol. *3*, 210–219.

Markowitz, V.M., Chen, I.-M.A., Palaniappan, K., Chu, K., Szeto, E., Pillay, M., Ratner, A., Huang, J., Woyke, T., Huntemann, M., et al. (2014). IMG 4 version of the integrated microbial genomes comparative analysis system. Nuc. Acids Res. *42*, D560–D567.

Martens, E.C., Chiang, H.C., and Gordon, J.I. (2008). Mucosal glycan foraging enhances fitness and transmission of a saccharolytic human gut bacterial symbiont. Cell Host Microbe *4*, 447–457.

Martens, E.C., Koropatkin, N.M., Smith, T.J., and Gordon, J.I. (2009). Complex glycan catabolism by the human gut microbiota: the Bacteroidetes Sus-like paradigm. J. Biol. Chem. *284*, 24673–24677.

Martens, E.C., Lowe, E.C., Chiang, H., Pudlo, N.A., Wu, M., McNulty, N.P., Abbott, D.W., Henrissat, B., Gilbert, H.J., Bolam, D.N., and Gordon, J.I. (2011). Recognition and degradation of plant cell wall polysaccharides by two human gut symbionts. PLoS Biol. *9*, e1001221.

Martinez-Jéhanne, V., du Merle, L., Bernier-Fébreau, C., Usein, C., Gassama-Sow, A., Wane, A.A., Gouali, M., Damian, M., Aïdara-Kane, A., Germani, Y., et al. (2009). Role of deoxyribose catabolism in colonization of the murine intestine by pathogenic Escherichia coli strains. Infect. Immun. *77*, 1442–1450.

McConnell, R.E., Higginbotham, J.N., Shifrin, D.A., Jr., Tabb, D.L., Coffey, R.J., and Tyska, M.J. (2009). The enterocyte microvillus is a vesicle-generating organelle. J. Cell Biol. *185*, 1285–1298.

McLeod, A., Snipen, L., Naterstad, K., and Axelsson, L. (2011). Global transcriptome response in Lactobacillus sakei during growth on ribose. BMC Microbiol. *11*, 145.

McNulty, N.P., Wu, M., Erickson, A.R., Pan, C., Erickson, B.K., Martens, E.C., Pudlo, N.A., Muegge, B.D., Henrissat, B., Hettich, R.L., and Gordon, J.I. (2013). Effects of diet on resource utilization by a model human gut microbiota containing Bacteroides cellulosilyticus WH2, a symbiont with an extensive glycobiome. PLoS Biol. *11*, e1001637.

Ndeh, D., Rogowski, A., Cartmell, A., Luis, A.S., Baslé, A., Gray, J., Venditto, I., Briggs, J., Zhang, X., Labourel, A., et al. (2017). Complex pectin metabolism by gut bacteria reveals novel catalytic functions. Nature *544*, 65–70.

Palchevskiy, V., and Finkel, S.E. (2009). A role for single-stranded exonucleases in the use of DNA as a nutrient. J. Bacteriol. *191*, 3712–3716.

Pan, N., and Imlay, J.A. (2001). How does oxygen inhibit central metabolism in the obligate anaerobe Bacteroides thetaiotaomicron. Mol. Microbiol. *39*, 1562–1571.

Parkin, D.W., Horenstein, B.A., Abdulah, D.R., Estupiñán, B., and Schramm, V.L. (1991). Nucleoside hydrolase from Crithidia fasciculata. Metabolic role,

purification, specificity, and kinetic mechanism. J. Biol. Chem. *266*, 20658–20665.

Petersen, C., and Møller, L.B. (2001). The RihA, RihB, and RihC ribonucleoside hydrolases of Escherichia coli. Substrate specificity, gene expression, and regulation. J. Biol. Chem. *276*, 884–894.

Pettolino, F.A., Walsh, C., Fincher, G.B., and Bacic, A. (2012). Determining the polysaccharide composition of plant cell walls. Nat. Protoc. *7*, 1590–1607.

Pluvinage, B., Grondin, J.M., Amundsen, C., Klassen, L., Moote, P.E., Xiao, Y., Thomas, D., Pudlo, N.A., Anele, A., Martens, E.C., et al. (2018). Molecular basis of an agarose metabolic pathway acquired by a human intestinal symbiont. Nat. Commun. *9*, 1043.

Pokusaeva, K., Neves, A.R., Zomer, A., O'Connell-Motherway, M., MacSharry, J., Curley, P., Fitzgerald, G.F., and van Sinderen, D. (2010). Ribose utilization by the human commensal Bifidobacterium breve UCC2003. Microb. Biotechnol. *3*, 311–323.

Porter, N.T., and Martens, E.C. (2017). The Critical Roles of Polysaccharides in Gut Microbial Ecology and Physiology. Annu. Rev. Microbiol. *71*, 349–369.

Pudlo, N.A., Urs, K., Kumar, S.S., German, J.B., Mills, D.A., and Martens, E.C. (2015). Symbiotic Human Gut Bacteria with Variable Metabolic Priorities for Host Mucosal Glycans. MBio *6*, e01282-15.

Rogowski, A., Briggs, J.A., Mortimer, J.C., Tryfona, T., Terrapon, N., Lowe, E.C., Baslé, A., Morland, C., Day, A.M., Zheng, H., et al. (2015). Glycan complexity dictates microbial resource allocation in the large intestine. Nat. Commun. *6*, 7481.

Sonnenburg, J.L., Xu, J., Leip, D.D., Chen, C.H., Westover, B.P., Weatherford, J., Buhler, J.D., and Gordon, J.I. (2005). Glycan foraging in vivo by an intestine-adapted bacterial symbiont. Science *307*, 1955–1959.

Sonnenburg, E.D., Zheng, H., Joglekar, P., Higginbottom, S.K., Firbank, S.J., Bolam, D.N., and Sonnenburg, J.L. (2010). Specificity of polysaccharide use in intestinal bacteroides species determines diet-induced microbiota alterations. Cell *141*, 1241–1252.

Speer, M.A. (2013). Development of a genetically modified silage inoculant for the biological pretreatment of lignocellulosic biomass. A Dissertation In Agricultural and Biological Engineering. https://etda.libraries.psu.edu/files/final_submissions/7579.

Temple, M.J., Cuskin, F., Baslé, A., Hickey, N., Speciale, G., Williams, S.J., Gilbert, H.J., and Lowe, E.C. (2017). A Bacteroidetes locus dedicated to fungal 1,6-β-glucan degradation: Unique substrate conformation drives specificity of the key endo-1,6-β-glucanase. J. Biol. Chem. *292*, 10639–10650.

Terrapon, N., Lombard, V., Drula, É., Lapébie, P., Al-Masaudi, S., Gilbert, H.J., and Henrissat, B. (2018). PULDB: the expanded database of Polysaccharide Utilization Loci. Nucleic Acids Res. *46* (D1), D677–D683.

Weickmann, J.L., Olson, E.M., and Glitz, D.G. (1984). Immunological assay of pancreatic ribonuclease in serum as an indicator of pancreatic cancer. Cancer Res. *44*, 1682–1687.

Wu, Z.L. (2011). Phosphatase-coupled universal kinase assay and kinetics for first-order-rate coupling reaction. PLoS One *6*, e23172.

STAR★METHODS

KEY RESOURCES TABLE

REAGENT or RESOURCE	SOURCE	IDENTIFIER
Bacterial Strains		
All bacterial strains are listed in Table S6		N/A
Oligonucleotides		
All oligonucleotides used in the study arelisted in Table S6		N/A
Chemicals and Recombinant Proteins		
1-Butanol	Sigma-Aldrich	Cat#360465
2-Deoxy-D-ribose	Sigma-Aldrich	Cat#31170
4-nitrophenyl N-acetyl-α-D-galactosamide	Sigma-Aldrich	Cat#N4264
4-nitrophenyl N-acetyl-β-D-glucosaminide	Sigma-Aldrich	Cat#N9376
4-nitrophenyl α-D-galactopyranoside	Sigma-Aldrich	Cat#N0877
4-nitrophenyl α-D-glucopyranoside	Sigma-Aldrich	Cat#N1377
4-nitrophenyl α-D-mannopyranoside	Sigma-Aldrich	Cat#N2127
4-nitrophenyl α-D-xylopyranoside	Sigma-Aldrich	Cat#N1895
4-nitrophenyl α-L-arabinofuranoside	Sigma-Aldrich	Cat#N3641
4-nitrophenyl α-L-arabinopyranoside	Sigma-Aldrich	Cat#N3512
4-nitrophenyl α-L-fucopyranoside	Sigma-Aldrich	Cat#N3628
4-nitrophenyl α-L-rhamnopyranoside	Sigma-Aldrich	Cat#N7763
4-nitrophenyl β-D-galactopyranoside	Sigma-Aldrich	Cat#N1252
4-nitrophenyl β-D-glucopyranoside	Sigma-Aldrich	Cat#N7006
4-nitrophenyl β-D-glucuronide	Sigma-Aldrich	Cat#N1627
4-nitrophenyl β-D-mannopyranoside	Sigma-Aldrich	Cat#N1268
4-nitrophenyl β-D-xylopyranoside	Sigma-Aldrich	Cat#N2132
4-nitrophenyl β-L-fucopyranoside	Sigma-Aldrich	Cat#N2505
5-Methyl-Uridine	Tokyo Chemical Industry (TCI)	Cat#M1405
Acetic acid, glacial	Sigma-Aldrich	Cat#338826
Acetic acid	Sigma-Aldrich	Cat#320099
Acetic acid, Optima LC/MS Grade	Fisher Scientific	Cat#A11350
Acetic anhydride	EMD Millipore	Cat#AX0080
Acetone	Fisher Scientific	Cat#A18P
Adenosine	Sigma-Aldrich	Cat#A9251
Adenosine 5′-monophosphate (AMP) disodium salt	Sigma-Aldrich	Cat#01930
ADP-Glucose (sodium salt)	Cayman Chemical	Cat#13139
AICAR	TOCRIS Bioscience	Cat#2840
Alkaline Phosphatase, Calf Intestinal (CIP)	NEB	Cat#M0290S
Ammonium hydroxide	Macron	Cat#3256
Amygdalin	Sigma-Aldrich	Cat#A6005
Amylopectin (maize)	Sigma-Aldrich	Cat#10120
Amylopectin (potato)	Sigma-Aldrich	Cat#A8515
Arabinan (sugar beet)	Megazyme	Cat#P-ARAB
Arabinogalactan (larch wood)	Megazyme	Cat#P-ARGAL
Boric acid	Sigma-Aldrich	Cat#B6768

(*Continued on next page*)

Continued

REAGENT or RESOURCE	SOURCE	IDENTIFIER
Brain heart infusion (Bacto)	Becton Dickinson	Cat#237500
Chloroform	Sigma-Aldrich	Cat#496189
Chondroitin sulfate	Sigma-Aldrich	Cat#C9819
Cytidine	Sigma-Aldrich	Cat#C4654
D-Arabinose	Sigma-Aldrich	Cat#10850
Deoxyadenosine monohydrate	Sigma-Aldrich	Cat#D7400
Deoxycytidine	Sigma-Aldrich	Cat#D3897
Deoxyinosine	Sigma-Aldrich	Cat#D5287
Deoxyuridine	Sigma-Aldrich	Cat#D5412
Dextran	Sigma-Aldrich	Cat#31389
Dichloromethane	Sigma-Aldrich	Cat#270997
D-Fructose	Sigma-Aldrich	Cat#F0127
D-Lyxose	Acros Organics	Cat#205230050
D-Rhamnose	Sigma-Aldrich	Cat#R3875
D-Mannose	Acros Organics	Cat#150601000
D-Melezitose	Sigma-Aldrich	Cat#M5375
D-Psicose	Tokyo Chemical Industry (TCI)	Cat#P1699
D-Ribose	Sigma-Aldrich	Cat#R7500
D-Ribose 1-phosphate bis(cyclohexylammonium) salt	Sigma-Aldrich	Cat#83866
D-Ribose 5-phosphate disodium salt dihydrate	Sigma-Aldrich	Cat#83875
5-Phospho-D-Ribose 1-diphosphate (PRPP) (sodium salt)	Cayman Chemical	Cat#18897
2'-Deoxyribose 1-phosphate bis(cyclohexylammonium) salt	Sigma-Aldrich	Cat#D6539
2'-Deoxyribose 5-phosphate sodium salt	Sigma-Aldrich	Cat#D3126
D-Tagatose	Sigma-Aldrich	Cat#T2751
D-Xylose	Sigma-Aldrich	Cat#X1500
Ethanolamine Hydrochloride	Sigma-Aldrich	Cat#E6133
Erlose	Sigma-Aldrich	Cat#E1895
EST-L Low Concentration Tuning Mix	Agilent Technologies	Cat#G1969-85000
Fiber-rich diet (rodent breeder diet)	LabDiet	Cat#5013
Galactose	Sigma-Aldrich	Cat#G0625
Galacturonic acid	Sigma-Aldrich	Cat#73960
Glucosamine hydrochloride	Sigma-Aldrich	Cat#G4875
Glucuronic acid	Sigma-Aldrich	Cat#G8645
Glycogen	Sigma-Aldrich	Cat#G0885
Hyaluronin	Sigma-Aldrich	Cat#53747
Isopropanol LC/MS Grade	Fisher Scientific	Cat#A461
Isopropanol	Sigma-Aldrich	Cat#I9030
Mucin O-glycans	Sigma-Aldrich	Custom extraction from Cat#M1778
N-acetyl galactosamine	Sigma-Aldrich	Cat#A2795
N-acetyl glucosamine	Sigma-Aldrich	Cat#A3286
Levan	Sigma-Aldrich	Cat#L8647
Heparin	Sigma-Aldrich	Cat#H4784
Glucose	Sigma-Aldrich	Cat#158968
Guanosine	Sigma-Aldrich	Cat#G6264

(*Continued on next page*)

Continued

REAGENT or RESOURCE	SOURCE	IDENTIFIER
Hypoxanthine	Sigma-Aldrich	Cat#H9636
InfinityLab Deactivator Additive	Agilent Technologies	Cat#5191-3940
Inosine	Sigma-Aldrich	Cat#I4125
Lactose	Sigma-Aldrich	Cat#L3750
L-Arabinose	Sigma-Aldrich	Cat#A3256
Low-fiber diet	Harlan Laboratories	Cat#TD.130343
Maltose Monohydrate	Sigma-Aldrich	Cat#M5885
Myo-Inositol	Sigma-Aldrich	Cat#I5125
N-acetylmuramic acid	Sigma-Aldrich	Cat#A3007
Neomycin Sulfate	Fisher Scientific	Cat#BP26695
Orcinol	Sigma-Aldrich	Cat#O1875
Palatinose hydrate	Sigma-Aldrich	Cat#P2007
Pectic galactan (potato)	Megazyme	Cat#P-PGAPT
Phenol pH 8 [For DNA extraction]	Sigma-Aldrich	Cat#P4557
Phenol:Chloroform:Isoamyl Alcohol	Fisher Scientific	Cat#BP1754I
Platinum Pfx DNA Polymerase	Invitrogen	Cat#11708013
p-nitrophenyl β-D-ribofuranoside	Sigma-Aldrich	Cat#43188
Pullulan	Sigma-Aldrich	Cat#P4516
D-Raffinose pentahydrate	Sigma-Aldrich	Cat#R0250
Rhamnogalacturonic acid I (potato)	Megazyme	Cat#P-RHAM1
Rebauside A	Sigma-Aldrich	Cat#1432
Ribitol (Adonitol)	Sigma-Aldrich	Cat#A5502
Ribonucleic Acid (RNA) from torula yeast Type VI	Sigma-Aldrich	Cat#R6625
Ribostymycin sulfate salt	Sigma-Aldrich	Cat#R2255
RNAprotect	QIAGEN	Cat#76506
RNase A	Sigma-Aldrich	Cat#R4875
Salmon Sperm DNA	Sigma-Aldrich	Cat#D1626
Sodium acetate	Sigma-Aldrich	Cat#S2889
Sodium borodeuteride	Sigma-Aldrich	Cat#205591
Sodium dodecyl sulfate	Sigma-Aldrich	Cat#L3771
Sodium hydroxide	Sigma-Aldrich	Cat#S845
Sorbitol	Fisher Scientific	Cat#BP439
Stachyose Hydrate	Sigma-Aldrich	Cat#S4001
Sucrose	Fisher Scientific	Cat#BP220
D-Tagatose	Sigma-Aldrich	Cat#T2751
Thymidine	Sigma-Aldrich	Cat#T1895
Trehalose dihydrate	Sigma-Aldrich	Cat#T9531
Tributylamine, 99%	Acros Organics	Cat#AC13932
Trifluoroacetic acid	Sigma-Aldrich	Cat#T6508
Tryptone	Fisher Scientific	Cat#BP1421
D-Turanose	Sigma-Aldrich	Cat#2754
UDP (sodium salt)	Cayman Chemical	Cat#18137
UDP-N-acetyl-D-Glucosamine (sodium salt)	Cayman Chemical	Cat#20353
UDP-α-D-Galactose Disodium Salt	Calbiochem	Cat#670111
UDP-α-Glucose	Cayman Chemical	Cat#15602
UDP-β-Glucose	Cayman Chemical	Cat#21620
Uridine	Sigma-Aldrich	Cat#U3003

(*Continued on next page*)

Continued

REAGENT or RESOURCE	SOURCE	IDENTIFIER
Uridine-5′-diphosphoglucuronic acid (sodium salt)	Cayman Chemical	Cat#20674
Xanthosine dihydrate	Sigma-Aldrich	Cat#X0750
Yeast Extract	Fisher Scientific	Cat#BP1422
Dnase I	NEB	Cat#M0303
Hot Start Taq	NEB	Cat#M0495
10X Thermopol® Reaction Buffer	NEB	Cat#B9004
dNTPs	Invitrogen	Cat#10297018
MgSO4	NEB	Cat#B1003
RbsK Recombinant Protein	MyBioSource	Cat#MBS1212370
Commercial Assays		
Universial Kinase Activity Kit	R&D Systems	Cat#EA004
SYBR Green I	Lonza	Cat#50513
DNeasy Blood & Tissue Kit	QIAGEN	Cat#69504
KAPA SYBR FAST qPCR Master Mix	KAPA Biosystems	Cat#KK4601
MinElute PCR Purification Kit	QIAGEN	Cat#28006
Ribo-Zero rRNA Removal Kits (Bacteria)	Illumina	Cat#MRZB12424
RNA Clean and Concentrator-5	Zymo Research	Cat#R1015
RNeasy Mini Kit	QIAGEN	Cat #74106
Superscript III Reverse Transcriptase	Thermo Fisher Scientific	Cat#18080093
TURBO DNA-free Kit	Ambion [Thermo Fisher Scientific]	Cat#AM1907
Software and Algorithms		
Arraystar	DNASTAR	https://www.dnastar.com/software/genomics/
Integrated Microbial Genomes database	Markowitz et al., 2014	https://img.jgi.doe.gov/
SeqMan Pro	DNASTAR	https://www.dnastar.com/software/molecular-biology/
EditSeq	DNASTAR	N/A
PrimerSelect	DNASTAR	N/A
Prism version 8	GraphPad	N/A
Agilent Masshunter Workstation version B.08.02	Agilent Technologies	N/A
Other (Essential Equipment)		
Anaerobic chamber	Coy manufacturing	Vinyl Type A + Type B
Automated plate handling device	Biotek Instruments	BIOSTACK2WR
Bead beater	Biospec Products	Mini-BeadBeater 16
Microtiter plate absorbance reader	Biotek Instruments	Synergy HT
Microtiter plate absorbance reader	Biotek Instruments	PowerWave HT
qPCR thermocycler	Eppendorf	Mastercycler ep realplex
Ultra Cruz UV Plate, 96 well, Flat Bottom	Santa Cruz Biotechnology	Cat#sc-213228
Gas Chromatography Instrument	Agilent Technologies	Model 7890A
Mass Spectrometer	Agilent Technologies	Model 5975C
Fused Silica Capillary Column (60 m x 0.25mm x 0.2μm)	Supelco Analytical	Cat#SP-2330
Triple Quadrupole 6470 Mass Spectrometer	Agilent Technologies	Model 6470
ZORBAX RRHD Extend-C18 Column (2.1 m x 150mm x 1.8μm)	Agilent Technologies	Cat#759700-902
ZOBAX Extend Fast Guard	Agilent Technologies	Cat#823750-937
1290 Infinity II Multicolumn Thermostat	Agilent Technologies	Cat#G7116B

(*Continued on next page*)

Continued		
REAGENT or RESOURCE	SOURCE	IDENTIFIER
1290 Infinity II Multisampler	Agilent Technologies	Cat#G7167B
1290 Infinity II LC Flexible Pump (Quaternary Pump)	Agilent Technologies	Cat#G7104A
Deposited Data		
Glucose Replicate #1	This study	GEO: GSM4081867
Glucose Replicate #2	This study	GEO: GSM4081868
Glucose Replicate #3	This study	GEO: GSM4081869
Ribose Replicate #1	This study	GEO: GSM4081870
Ribose Replicate #2	This study	GEO: GSM4081871
Ribose Replicate #3	This study	GEO: GSM4081872

LEAD CONTACT AND MATERIALS AVAILABILITY

This study did not generate new or unique reagents other than genetic deletions within the strain *Bacteroides thetaiotaomicron* ATCC 29148 (VPI-5482). All requests for these mutant strains, protein constructs, or expressing strains or any other questions about methods or reagents used in this study will be available through directing inquiries to the Lead Contact, Eric C. Martens (emartens@umich.edu).

EXPERIMENTAL MODEL AND SUBJECT DETAILS

Gnotobiotic Mouse Experiments

All experiments involving animals, including euthanasia via carbon dioxide asphyxiation, were approved by the University Committee on Use and Care of Animals at the University of Michigan (NIH Office of Laboratory Animal Welfare number A3114-01) and overseen by a veterinarian. Six to eight-week-old, germfree female Swiss-Webster mice were initially maintained on the standard, fiber-rich lab diet (LabDiet 5010, LabDiet, St. Louis, MO), where appropriate, mice were switched to a fiber-free diet (Envigo-Teklad TD 130343) and maintained for one week prior to colonization with *Bt* strains. After stable colonization had been observed, at day 14 some groups of mice were provided water ab libitum containing one of the following: 1% ribose, 1% Nucleoside mixture (0.25% thymidine, 0.25% uridine, 0.25% 5-methyl uridine, and 0.25% cytidine) or Type VI torula yeast RNA. DNA was extracted from fecal pellets throughout the experiment and strain abundance was quantified as described previously (Desai et al., 2016). Relative abundance of each strain was normalized to the original abundance on day of gavage (day 0). Post-sacrifice, cecal contents were collected, flash frozen and stored at −80°C. RNA was extracted as described previously (Porter and Martens, 2017), briefly, RNA was phenol-chloroform treated and ethanol precipitated, DNA removed by treatment with TURBO^{TM} DNaseI (Ambion), followed by purification using RNeasy mini kit (QIAGEN) according to manufactures instructions.

Bacterial Strains, Culturing Conditions, and Molecular Genetics

B. thetaiotaomicron ATCC 29148 (VPI-5482) and its genetic variants, as well as other *Bacteroides* strains used in this study, were routinely grown in tryptone-yeast extract-glucose (TYG) broth medium (Holdeman, 1977), in minimal medium (MM), plus a defined carbon source (Martens et al., 2008), or on brain heart infusion agar with 10% defibrinated horse blood (Colorado Serum Co.). Unless otherwise noted, carbon sources used in MM were added to a final concentration of 5 mg/mL. Cultures were grown at 37°C in an anaerobic chamber (10% H_2, 5% CO_2, and 85% N_2; Coy Manufacturing, Grass Lake, MI). Genetic deletions and mutations were performed by counter-selectable allelic exchange as previously described (Koropatkin et al., 2008). Complementation of deletion strains was performed using pNBU2 vectors as described previously (Martens et al., 2008), containing 314 bp upstream of *BT2802*, predicted to contain the promoter sequence for the Δ*rusR* strain or 186 bp upstream of *BT2803-04* containing the entire intergenic region for the Δ*rusK1/K2* strain. Primers used in this study are listed in Table S6 To quantify growth on carbon sources and examine mutant phenotypes, increase in culture absorbance (600 nm) in 200μl cultures in 96-well plates was measured at 10 min intervals for at least 96 h on an automated plate reader as previously described (Martens et al., 2011). To achieve consistent and robust growth on nucleosides and other covalently linked sources of ribose, free ribose was added at a final concentration of 0.5 mg/mL to MM containing 5 mg/mL of carbon source. Growth on 5mg/mL of MM containing Type IV Torula yeast RNA (Sigma) was obtained by adding 100 units of calf-intestinal alkaline phosphatase (CIP) (New England Biolabs) and 2mg/mL RNase A (Sigma). Growth parameters and conditions for all substrates are summarized in Table S1.

METHOD DETAILS

Genetic Manipulation and Recombinant Protein Purification in *E. coli*

To create a nucleoside hydrolase-free expression background, *E. coli* BL21-AI™ One Shot® cells (Invitrogen) were manipulated using lambda red recombineering to introduce genetic deletions of the ribose-inducible hydrolase genes (*rih*) to avoid contaminating activity in downstream applications of purified proteins (Petersen and Møller, 2001). The *E. coli* gene deletion procedure developed by Datsenko and Wanner (Datsenko and Wanner, 2000) was followed with few modifications. Briefly, BL21-AI cells were transformed with the pKD46 plasmid. Transformed cells were grown overnight in LB + Amp^{100} and sub-cultured, when the culture absorbance (600 nm) reached 0.1, L-arabinose was added to 10 mM final concentration to induce the P_{BAD} promoter of pKD46, cells were allowed to grow to an OD between 0.6-0.8 and made competent for electroporation by cold water washes and stored in 10% glycerol aliquots. For recombineering, 400ng of gel-purified PCR product was added to freshly made cells and incubated for 10 min on ice, electroporated in a 2mm gap cuvette at 2500 V, recovered in 1 mL LB at 30°C for 5 h. All knockouts were made sequentially in this manner via introduction of the following antibiotic cassettes (spectinomycin from K11497 for Δ*rihA*; hygromycin from K11521 for Δ*rihB*; gentamicin from K11590 for Δ*rihC*), and the following concentrations of antibiotic were used for selection: $Spec^{80}$, $Hygro^{200}$, $Gent^{10}$. Following construction of the last deletion, the pKD46 plasmid was heat-cured by passaging twice at 42°C in LB. To better control background expression of the T7 promoter, the T7 lysozyme containing plasmid, pLysS from BL21 (DE3) (Lucigen) was introduced into the strain via Ca^{2+} chemical competence/heat shock. Protein purification was accomplished using the pETite N-His vector (Lucigen). PCR primers were designed to amplify products for BT2803, BT2804, BT2807 and BT2808 containing all amino acids for BT2804 residues 1-311, or all amino acids downstream of the predicted signal peptide sequences, residues 22-539 for BT2807 and residues 22-338 for BT2808, for BT2803 two constructs were made containing either all amino acids 1-321 or a construct based on an alternative start site containing residues 15-321 (only this construct produced robust expression, while the full length failed to provide active product or good expression), amplified and transformed into Hi-Control 10G cells according to manufactures protocol (Lucigen, *Expresso*™ T7 cloning and expression system). pETite plasmids containing BT2803, BT2804, or BT2807 were transformed into *E. coli* strains TUNER or for BT2808 into BL21-AI Δ*rihABC* + pLysS. A single colony was grown in 5 mL of LB+Kan^{50} for 16 h. This pre-inoculum was added to to 1L of Terrific-Broth with 50ng/ul of Kanamycin and 10 ng/ul of Chloramphenicol (BT2808) or 50ng/ul of Kanamycin (BT2807) and culture was grown with shaking at 37°C until absorbance 0.4 at 600nm. BT2807 and BT2808 cells were induced with a final concentration of 0.2mM or 1 mM IPTG and 0.2% 20mM L-arabinose, respectively, and temperature was reduced to 16°C and outgrown overnight. The recombinant proteins were purified by immobilized metal ion affinity chromatography using cobalt (BT2807) or nickel-affinity (BT2808) columns was accomplished as described previously (Cameron et al., 2014).

Measurements of Transcriptional Responses by qPCR

Bt and other *Bacteroides* strains were grown to mid-exponential phase 0.6-0.8 (absorbance at 600nm) in MM-ribose, MM-arabinose, MM-xylose, or MM-glucose, two volumes of RNA protect added, followed by centrifugation and storage of cell pellets at −80°C. Total RNA was extracted using the RNeasy mini kit buffers (QIAGEN) and purified on RNA-binding spin columns (Epoch), treated with TURBO DNaseI (Ambion) or DNase I (NEB) after elution and purified again using a second RNeasy mini kit isolation column. Reverse transcription was performed using SuperScript III reverse transcriptase and random primers (Invitrogen). The abundance of each target transcript in the resulting cDNA was quantified using either KAPA SYBR® FAST qPCR mix (KAPA Biosystems) or a homemade qPCR mix as described previously (Speer, 2013). Each 20 uL reaction contained 1X Thermopol Reaction Buffer (NEB), 125uM dNTPs, 2.5mM MgSO4, 1X SYBR Green I (Lonza), 500nM gene specific or 65nM 16S rRNA primer and 0.5 units Hot Start *Taq* Polymerase (NEB), and 10ng of template cDNA. For the KAPA mix, 400 nM of primers specific for genes in the *rus* locus of *Bt* or the *rusC*-like gene of other *Bacteroides* species or 62.5 nM of 16S rRNA primers and 10ng of template cDNA as described previously (Pudlo et al., 2015). Using the ddCT method, raw values were normalized to 16S rRNA values and then MM+ribose values were referenced to the values obtained in MM-glucose to obtain a fold-change. Measurements of transcriptional response over time in MM-ribose or nucleosides was performed similarly to previously described (Cameron et al., 2014). Briefly, strains were grown in TYG, subcultured 1:50 into MM-glucose, at mid-exponential phase, cells were washed twice in MM-no carbon and resuspended in MM-ribose with time points being taken every 5 min for the first 30 min and every 15 min for a total of 120 min. Measurements of transcriptional responses to varying amounts of ribose were performed similarly as above, but only one time point was taken after 30 min of exposure to varying concentration of MM-ribose ranging from 0.0005 mg/mL to 5mg/mL.

Antibody Production, Western Blotting and Immunofluorescent Microscopy

Purified recombinant BT2807 and BT2808 proteins were used as antigens to raise rabbit polyclonal antibodies (Cocalico Biologicals, Inc, Stevens PA). Antibody specificity and cellular localization for BT2807 and BT2808 were determined by western blotting of wild-type and relevant mutant strains and by immunofluorescent microscopy of *Bt* VPI-5482 grown in MM+glucose or MM+ribose. Growth conditions are described above, cells for WB were grown to mid-log optical absorbance (600 nm) 0.6-0.7 or 0.4-0.5 for IF. Western blots of *Bt* whole cell lysates were performed using the primary, polyclonal antibodies mentioned above and secondary antibody conjugated to goat anti-Rabbit IgG conjugated alkaline phosphatase (Sigma) and detected with NBT/BCIP (Roche). Surface expression of BT2807 or BT2808 was examined by staining with a BT2807- or BT2808-specific primary antibody in non-permeabilized formaldehyde-fixed *Bt* cells and detected with Alexa-Flour® 488 conjugated goat anti-Rabbit IgG secondary (Molecular

Probes), as described previously (Cameron et al., 2014). Cells were imaged on an IX-70 inverted microscope (Olympus) with images captured at 100x magnification. A minimum of five fields of view per slide was observed with n = 2 biological replicates.

Functional Annotation and Comparative Genomics of *rus* PULs across Bacteroidetes Genomes

Initial functional annotations of *Bt rus* genes were taken from the Integrated Microbial Genomes (IMG) database using the Pfam, InterPro, COG, or KOG predictions. In cases where multiple annotations, we selected the more inclusive terms (e.g., nucleoside phosphorylase instead of purine or pyrimidine-specific nucleoside phosphorylase). A total of 354 different *Bacteroidetes* strains were tested for growth on ribose as a sole carbon source as shown in Figure 6A and summarized in Table S4. The ability to use ribose is shown in the context of a previously published human gut Bacteroidetes phylogeny that used 14 conserved genes across phylum members (Larsbrink et al., 2014). To search for *rus* locus homologs across the Bacteroidetes phylum, we used the amino acid sequences of the *rusK1, rusK2, rusT,* and *rusR* genes from the *Bt* type strain as deletion of these genes yielded growth defects on ribose. We searched the IMG database (current as of May 2018) and performed phylum-level BLAST searches with an E-value cutoff of 1e-50. We chose this stringent cutoff as initial searches using lower values obtained many non-specific hits of genes encoding other kinases and permeases that did not appear to be specific for ribose, including in the *Bt* VPI-5482 genome for which Rusk1 and RusK1 are the only kinases able to promote ribose growth. After we completed our search for *rusK, rusT,* and *rusR* homologs we used the Gene Neighborhood tool in IMG to determine if these hits were located directly next to other genes involved in ribose utilization. The presence of a minimum of two adjacent *rus* gene homologs was required to count the presence of a candidate utilization locus. Following this first round of searching we observed that many of the *rus* loci contained one or more nucleoside cleaving enzymes such as homologs of *Bt rusNH* or ADP-ribosylglycohydrolases (RGH) and upstream putative regulatory genes. To give our search more power and potentially find additional *rus* homologs we performed additional searches with the same E-value threshold for homologs of *Bt rusNH,* or homologs of the ADP-RGH in *B. xylanisolvens XB1A*. When assembling the comparative genomics data, gene names and glycoside hydrolase family assignments are shown as predicted within IMG by either annotation, Pfam and/or InterPro predictions or confirmed by BLAST of the amino acid sequence of individual genes. Further, in refinement, a handful of genes were found below our E-value, but included in the table as it is clear from gene neighborhood views in IMG that it is likely part of a *rus* locus due to adjacent hits of *rus* homologs. Types of *rus* have been assigned based only on gene content and arrangement as a way to indicate differences, however subtle. In completing our table we have included the bit score as well as the amino acid % identities compared to *Bt rus* genes or *Bx XB1A* ADP-RGH genes. All of the positive gene hits with locus tag information, isolation location, and other relevant strain information is summarized in Table S5.

RNaseq Analysis

To determine the global transcriptional response to growth in ribose as the sole carbon source, *Bt* cells were grown overnight in rich TYG media then transferred to fresh MM containing either 5 mg/mL glucose or 5 mg/mL ribose. Cells were then grown until mid-log phase (absorbance between 0.6-0.8) and two volumes of RNA Protect (QIAGEN) were added to cells. RNA was isolated as described above and purified whole RNA was then rRNA depleted using the Ribo-Zero Bacterial rRNA Removal Kit (Illumina Inc.) and concentrated with the RNA Clean and Concentrator-5 kit (Zymo Research Corp, Irvine, CA). Samples were multiplexed for sequencing on the Illumina HiSeq platform at the University of Michigan Sequencing Core. Data was analyzed using Arraystar software (DNASTAR, Inc.) using RPKM normalization with default parameters. Gene expression in ribose was compared to gene expression in a glucose reference. Genes with significant up- or downregulation were determined by the following criteria: genes with an average fold-change $\geq$ 5-fold and with at least 2/3 biological replicates with a normalized expression level $\geq$ 1% of the overall average RPKM expression level in either glucose or ribose, and a p value < 0.05 (t test with Benjamini-Hochberg correction) (Table S3).

Enzyme Assays

Recombinant proteins purified in *E. coli*, were used to determine enzyme kinetics for RusGH, RusNH, RusK1, and RusK2. For RusNH we used a *p*-nitrophenol-ribofuranoside substrate with absorbance readings at 405nm over a 24 h period as described previously (Desai et al., 2016), with modifications for using purified protein instead of crude extract, using 0.5mM of enzyme in a buffer containing 20mM HEPES and 100mM NaCl, at pH 6.7 at 37°C and continuous absorbance readings. For RusGH, a panel of other 4-nitrophenol based substrates in addition to *p*-NP-ribofuranoside were tested at pH 9.0 in 100 mM Tris at 37°C for 16 h with 1.5-15 μM of enzyme and using endpoint absorbance measurements. Ion requirements of the RusGH were assayed in *p*-NP-ribofuranoside by addition of divalent cations in the form of $CaCl_2$, $ZnCl_2$, or $MgCl_2$, at 2, 5, or 10 mM concentrations, or in the presence of 10 mM EDTA. Specificity and kinetic parameters for RusNH on natural nucleoside substrates were determined as described previously using a UV-based assay (Parkin et al., 1991). Briefly, a 96-well, UV-compatible microplate (Santa Cruz Biotechnologies) was used with substrate concentrations ranging from 0.025mM-2.5mM, and enzyme concentrations of 0.25-1uM. Assays were immediately read after addition of enzyme by continuous reading of absorbance at 262nm or 280nm with time points taken every 2.5 min over 12-24 h at 37°C. Volume was 250uL in all assays and carried out in buffer containing 20mM HEPES and 100mM NaCl, at pH 6.7, adjusted with acetic acid. As a measure of catalytic efficiency, (K_{cat}/K_M) was unable to be determined by classical Michaels-Menton kinetics as Vmax was never reached and therefore Km values were not accurate, so we used a previously established method of estimating this value (Ndeh et al., 2017). Briefly, we used a single substrate concentration to calculate (k_{cat}/K_M) and checked to be $< < K_M$ by halving and doubling the substrate concentration and observing a proportionate increase or decrease in rate. Therefore the equation, $V_0 = (k_{cat}/K_M)[S][E]$ was used to calculate k_{cat}/K_M in our case. For, RusGH a panel of other 4-nitrophenol based substrates in addition

to *p*-NP-ribofuranoside were tested at pH 9.0 in 100 mM Tris at 37°C for 16 h with 1.5-15 μM of enzyme with endpoint absorbance measurements. Ion requirements of the RusGH were assayed in *p*-NP-ribofuranoside by addition of divalent cations in the form of $CaCl_2$, $ZnCl_2$, or $MgCl_2$, at 2, 5, or 10 mM concentrations, or in the presence of 1 mM EDTA. The RusGH was tested against a panel of oligosaccharides, nucleosides and nucleotides. Briefly, the reactions were performed with 10 μM of RusGH, 8mg/mL substrate or 5mM monosaccharide in 50 mM TRIS pH 9.0 at 37°C for 16 h. A control reaction was performed in the same conditions without enzyme. The activity was qualitative determined by thin layer chromatography. 6 μL of the reaction was spotted on foil backed silica plate (Silicagel 60, 20 × 20, Merck) and develop in butanol:acetic acid:water 2:1:1 (mobile phase). The products of the reaction were detected by immersing the TLC plate in developer (sulphuric acid/ethanol/water 3:70:20 v/v, orcinol 1%) for 30 s and heating to 100°C for 2 min. A standard of ribose was run in all TLC plates. For RusK1/K2 a phosphatase-coupled, universal kinase assay was used according to manufacturer instructions to determine a specific activity of the kinases on pentose sugars. (R&D Systems, Minneapolis, MN) (Wu, 2011). Specifically, all reactions were carried out in buffer containing 70 mM Tris, 100 mM KCl, and 5 mM $MgCl_2$ at pH 7.5, this buffer is based on previous studies examining ribokinase activities and showing this buffer provided maximal enzymatic activity (Chuvikovsky et al., 2006). Reactions were carried out in 50 μL at 37°C for 30 min. All reactions contained 1 mM ATP, 100 ng of coupling phosphatase, and a range of enzyme concentrations ranging from 0.1-10 μM of RusK1, RusK2, or *E. coli* RbsK (MyBioSource, San Diego, CA), as a positive control, and for the acceptor substrate either 10 mM of ribose or deoxyribose or 200 mM of all other sugars tested including: arabinose, xylose, glucose or fructose etc. Determination of specific activity was based off of a coupling rate of 0.399 and a rate constant of 97.78 nmol/min/μg/mM (empirically determined by the kit manufacture). In brief, our specific activity is based on an endpoint observation across a minimum of 5 enzyme concentrations, the resulting absorbance is fit to a known phosphate standard curve equation and the resulting rate is nM (product formed)/min (held standard at 30 min)/uM enzyme/mM of substrate. This is the specific activity at a defined endpoint and so should not be confused with a rate taken at several enzyme concentrations over different time points, but rather used a crude measurement for which to compare different enzymes.

Determination of Free and Acid Hydrolysable Monosaccharide Content in Diets and Cecal Contents Using GC/MS

Prior to analysis, diets were ground to a fine powder using a blender followed by mortar and pestle, while cecal contents were dried by lyophilization. Samples were analyzed for free and linked monosaccharides using the following method described in (Pettolino et al., 2012). In brief, all reactions began with 1-3mg of sample and samples were hydrolyzed in 100ul of 2.5 M TFA for 90 min at 121°C. Samples were allowed to cool to room temperature (RT) and myo-inositol was added as an internal standard (20ul of 2.5mg/mL) and dried under nitrogen. 150ul of methanol was added, dried and repeated once more. Dried samples were then reduced by dissolving in 50ul of 2M NH_4OH followed by addition of 50 ul of freshly made 1M $NaDB_4$ in 2M NaOH. This mixture was sonicated in a water bath for 1 min, followed by incubation at room temperature for 2.5 h. 23ul of glacial acetic acid was added and samples dried and evaporated 2x with 250ul of 5% (v/v) acetic acid in methanol, followed by 2x evaporation with 250ul of methanol, drying after each step. Acetylation was done by addition of 250ul acetic anhydrate and sonicated 5 min followed by incubation at 100°C for 2.5 h. 2ml of ddH_2O was added and sample vortexed to dissolve residue, followed by room temperature incubation for 10 min. 1ml of dichloromethane (DCM) was added and vortexed followed by centrifugation at 2000 rpm for 2.5 min. The aqueous phase was discarded and the DCM phase washed 2x with 2 mL of ddH_2O. DCM phase was dried and residue dissolved in 250 ul acetone. For free monosaccharide analysis the initial hydrolysis step with TFA was not performed. To establish a limit of detection in cecal contents, varying amounts of ribose (0.00002-0.2 mg, in 10-fold increments) were added at the same time as the myo-inositol standard to establish percent recovery throughout the methods used. Acetylated samples were analyzed on a gas chromatography (Agilent Technologies model 7890A) coupled mass spectrometer (Agilent Technologies model 5975C) using a fused silica capillary column (60 m x 0.25 mm x 0.2μm SP-2330, Supelco Analytical).

LC/MS/MS Determination of Positional Ribose Phosphorylation by *rus* Ribokinases

Samples were prepared as follows with reactions containing the following: 1μM of either enzyme (RusK1 or RusK2), 10mM of a starting substrate (ribose, ribose 1-phosphate, or ribose 5-phosphate), 1mM ATP, with all components dissolved in a buffer containing 70 mM Tris, 100 mM KCl, and 5 mM $MgCl_2$ at pH 7.5and incubated at 37°C for 30 min. Reactions were then flash frozen and stored at −80°C until processing. For analysis, 100% MeOH was added to thawed samples in buffer at a 4:1 ratio to extract metabolites. Samples were then dried down and reconstituted in 45 μL of 1:1 MeOH/H_2O. Samples were run on a 6470 Series Agilent Technologies Triple Quadrupole Mass Spectrometer with Ion-Pairing chromatography. The acquisition method was programed to detect for dynamic multiple reaction monitoring (dMRM) of four compounds of interest: ribose, ribose 1-phosphate, ribose 5-phosphate, and ribose 1,5-bisphosphate. The dMRM scan is used with a 0.07 min peak width and acquisition time of 24 min. The detected fragments displayed the following dMRM transitions: ribose 149->89 at 1.31 min with collision energy (CE) of 5 eV; ribose-1-phosphate 229->210 at 9.4 min with CE of 9eV; ribose-5-phosphate 229-> 97 at 7.9 min with CE of 13eV; ribose-1,5-bisphosphate 309->211 at 14.6 min with CE of 13 eV. The following parameters were incorporated into the method: delta retention time of plus and minus 1 min, fragmentor of 40 eV and cell accelerator of 5 eV. Agilent Qualitative Analysis version 7.00 was used for post-acquisition analysis. Our empirically determined range of detection was established above a noise baseline determined by running enzyme, buffer, sample, and internal controls for each species of interest where we did not anticipate these species being detected. This was determined to be 10^3 which was our highest background reading (Table S2**e**). Detailed instrumentation running parameters are here described. The following solvents were used during processing, Solvent A: 97% H_2O and 3% MeOH, Solvent B: 15 mM acetic acid and 10 mM tributylamine at pH 5. Solvent C: 15 mM acetic acid and 10 mM tributylamine in MeOH. Washing Solvent D is 100% acetonitrile.

LC system seal washing solvent is 90% water and 10% isopropanol, while the needle washing solvent is 75% methanol and 25% water. The Agilent Technologies Triple Quad 6470 LC/MS system used here consists of 1290 Infinity II LC Flexible Pump (Quaternary Pump), 1290 Infinity II Multisampler, 1290 Infinity II Multicolumn Thermostat with 6 port valve and 6470 triple quadrupole mass spectrometer. Agilent Masshunter Workstation Software LC/MS Data Acquisition for 6400 Series Triple Quadrupole MS with Version B.08.02 is used for compound optimization and data acquisition. The following column was used for separation: Agilent ZORBAX RRHD Extend-C18, 2.1 × 150 mm, 1.8 um and ZORBAX Extend Fast Guards for UHPLC are used in the separation. LC gradient profile is: at 0.25 mL/min, 0-2.5 min, 100% A; 7.5 min, 80% A and 20% C; 13 min 55% A and 45% C; 20 min, 1% A and 99% C; 24 min, 1% A and 99% C; 24.05 min, 1% A and 99% D; 27 min, 1% A and 99% D; at 0.8 mL/min, 27.5-31.35 min, 1% A and 99% D; at 0.6 mL/min, 31.50 min, 1% A and 99% D; at 0.4 mL/min, 32.25-39.9 min, 100% A; at 0.25 mL/min, 40 min, 100% A. Column temperature is kept at 35°C, samples at 4°C, and injection volume is 2 μl. The 6470 Triple Quad MS was calibrated with ESI-L Low concentration Tuning mix. Source parameters: Gas temp 150°C, Gas flow 10 l/min, Nebulizer 45 psi, Sheath gas temp 325°C, Sheath gas flow 12 l/min, Capillary −2000 V, Delta EMV −200 V.

QUANTIFICATION AND STATISTICAL ANALYSIS

Student's t tests for *in vivo* data were performed for each time point in GraphPad Prism version 8.1 with a paired, two-tailed distribution. Detailed statistical information is included in the figure legends where appropriate.

DATA AND CODE AVAILABILITY

Data from this study have been deposited in the NCBI Gene Expression Omnibus (GEO) database under the following accession identifiers: RNA-seq data (GEO: GSM4081867, GSM4081868, GSM4081869, GSM4081870, GSM4081871, GSM4081872).